

CFHT Optical PDCS Survey II: Evolution in the Space Density of Clusters of Galaxies^{1,2}

B. P. Holden^{3,4}

Department of Astronomy and Astrophysics, University of Chicago

5640 South Ellis Ave. Chicago, Illinois 60637

holden@oddjob.uchicago.edu

C. Adami

Department of Physics and Astronomy, Northwestern University, 2131 Sheridan Road, Evanston, Illinois 60208-2900

IGRAP, Laboratoire d'Astronomie Spatiale, Traverse du Siphon, F-13012, Marseille, France

christophe.adami@astrsp-mrs.fr

R. C. Nichol

Department of Physics, Carnegie Mellon University, 5000 Forbes Ave. Pittsburgh, Pennsylvania 15213-3890

nichol@andrew.cmu.edu

F. J. Castander

Observatoire Midi-Pyrenees, 14, Avenue Edouard Belin, 31400 Toulouse, France
Department of Astronomy and Astrophysics, University of Chicago, 5640 South Ellis Ave. Chicago, Illinois 60637

fjc@ast.obs-mip.fr

L. M. Lubin

¹Based on observations collected at the Canada France Hawaii Telescope operated by the National Research Council of Canada, the Centre National de La Recherche Scientifique de France, and the University of Hawaii

²Based on observations obtained with the Apache Point Observatory 3.5-meter telescope, which is owned and operated by the Astrophysical Research Consortium

³Visiting Astronomer, Kitt Peak Observatory, National Optical Astronomy Observatories, which is operated by the Association of Universities for Research in Astronomy (AURA), Inc., under cooperative agreement with the National Science Foundation.

⁴Currently residing at: IGPP/UC-Davis, L-413, LLNL, P.O. 808, Livermore, CA 94551

*California Institute of Technology, 105-24 Caltech, 1201 East California Blvd, Pasadena,
California 91125*

`lml@astro.caltech.edu`

A. K. Romer³

*Department of Physics, Carnegie Mellon University, 5000 Forbes Ave. Pittsburgh, Pennsylvania
15213-3890*

`romer@andrew.cmu.edu`

A. Mazure

IGRAP, Laboratoire d'Astronomie Spatiale, Traverse du Siphon, F-13012, Marseille, France

`alain.mazure@astrsp-mrs.fr`

M. Postman^{3,5}

Space Telescope Science Institute⁵, 3700 San Martin Dr., Baltimore, Maryland 21218

`postman@stsci.edu`

and

M. P. Ulmer

*Department of Physics and Astronomy, Northwestern University, 2131 Sheridan Road, Evanston,
Illinois 60208-2900*

`m-ulmer2@nwu.edu`

ABSTRACT

We present the first dynamical study of the optically selected Palomar Distant Cluster Survey (PDCS). We have measured redshifts for seventeen clusters of galaxies in the PDCS and velocity dispersions for a subset of eleven. Using our new cluster redshifts, we re-determine the X-ray luminosities and upper limits. We show that eleven out of twelve PDCS clusters we observed are real over-densities of galaxies. Most clusters have velocity dispersions appropriate for clusters of galaxies. However, we find a fraction ($\sim \frac{1}{3}$) of objects in the PDCS which have velocity dispersions in the range of groups of

⁵The Space Telescope Science Institute is operated by the AURA, Inc., under National Aeronautics and Space Administration (NASA) Contract NAS 5-26555.

galaxies ($200 \text{ km s}^{-1} \pm 100 \text{ km s}^{-1}$) but have richnesses appropriate for clusters of galaxies.

Within our survey volume of $31.7_{-0.8}^{+0.5} \times 10^4 \text{ h}^{-3} \text{ Mpc}^3$ ($q_o = 0.1$) for Richness Class 2 and greater clusters, we measure the richness function, X-ray luminosity function (using both the detections and upper limits), and the mass function derived from our velocity dispersions. We confirm that the space density, as a function of richness, of clusters of galaxies in the PDCS is ~ 5 times that of the Abell catalog. Excluding the above fraction of $\frac{1}{3}$ of objects with low velocity dispersions, we measure a space density ~ 3 times that of the Abell catalog for equivalent mass clusters of galaxies, raising the possibility that the Abell catalog is incomplete. However, our space density estimates are in agreement with other low-redshift, optically-selected cluster surveys such as the EDCC, APM and EDCC2. Our X-ray luminosity function agrees with other measurements based on both X-ray and optically selected samples, so we find that the PDCS does not miss clusters of galaxies that would be found in an X-ray selected survey. Our resulting mass function, centered around $10^{14} M_{\odot} h^{-1}$, agrees with the expectations from such surveys as the Canadian Network for Observational Cosmology cluster survey, though errors on our mass measurements are too large to constrain cosmological parameters. We do show that future machine-based, optically-selected surveys can be used to constrain cosmological parameters.

1. Introduction

The space density of virialized clusters of galaxies as a function of mass and redshift are primary predictions of theories on the formation and evolution of structure. In general, three parameters control the shape, normalization and evolution of the mass function of clusters of galaxies. These parameters are the density of matter in the universe, Ω_m , the variance of the distribution of mass density fluctuations at cluster scales, σ_8 , and the shape of the spectrum of density fluctuations, commonly quantified as Γ (Press & Schechter 1974; Efstathiou et al. 1992; Lacey & Cole 1993; Viana & Liddle 1996; Eke et al. 1996; Kitayama & Suto 1997). We can directly test these theoretical predictions and, therefore, constrain these parameters, by measuring masses of clusters of galaxies in a sample with a known survey volume.

Most efforts to measure the space density of clusters of galaxies as a function of mass have focused on X-ray selected samples. X-ray selection has two advantages. First, X-ray luminosity is strongly correlated with mass. Second, X-ray selected surveys have a selection function that is easy to quantify. Therefore, previous work focused on the mass function derived from velocity dispersions of X-ray selected clusters (Carlberg et al. 1997a; Borgani et al. 1999a, as examples), the temperature function (Henry 1997, for an example) or the luminosity function (Reichart et al. 1999b; Borgani et al. 1999b, as examples).

There is a large spread in the above results. Yet, most of the papers mentioned above use the sample of clusters of galaxies from the Extended Medium Sensitivity Survey or EMSS (Gioia et al. 1990a,b; Henry et al. 1992; Nichol et al. 1997). For example, Reichart et al. (1999b) finds the most likely value of Ω_m from the mass function of the EMSS to be around 1, while the CNOC survey (Carlberg et al. 1996, for example) finds a the most likely value to be to 0.2. Recently, Borgani et al. (1999a) finds that Ω_m from the CNOC survey can be constrained to the range $0.35 < \Omega_m < 1.0$. Borgani et al. (1999a) finds that the large uncertainty in the best fitting values of Ω_m is partly the result of the uncertainty in the mass function of low redshift clusters of galaxies. However, the high redshift sample of the EMSS only contains the highest mass clusters and, furthermore, is incomplete even at those masses (see Borgani *et al.* 1999a for a discussion of the completeness of the sample used by Carlberg *et al.* 1997, Borgani *et al.* 1999a estimate that the CNOC sample contains only 25% of all clusters with $\sigma_v > 800 \text{ km s}^{-1}$ because of the X-ray threshold of $> 10^{45} \text{ erg s}^{-1}$). Though there is great potential in the CNOC sample, both a larger number of clusters and a larger range in masses at both high and low redshift is needed to constrain cosmological parameters.

To increase the range in mass at high redshift, we have used optically selected clusters of galaxies. Specifically, we have collected a number of redshift measurements towards clusters of galaxies in the Palomar Distant Cluster Survey (Postman et al. 1996, PDCS) so we can measure velocity dispersions, the first such velocity dispersion measurements of this catalog. With our sample of $0.2 \leq z \leq 0.6$ clusters of galaxies, we could potentially improve the sample of Carlberg et al. (1997a) and make a better measurement of the value of Ω_m . The PDCS contains a much larger space density of clusters of galaxies, between $\sim 10^{-5}$ and $\sim 10^{-6} \text{ h}^{-3} \text{ Mpc}^3$, in the same redshift range as the EMSS, and, therefore, should contain lower mass clusters. We should then have a sample that, when combined with the EMSS, increases the dynamic range of the cluster mass function making a more robust measurement of Ω_m .

The approach of the PDCS was to create a model of what clusters of galaxies look like, called a matched-filter. The model for the galaxy distribution is a Schechter function for the luminosity distribution of the cluster galaxies and a profile of $\frac{1}{\sqrt{1+(r/r_c)^2}}$. The core radius of the radial profile were fixed as were the slope and “knee” of the Schechter luminosity function. The total cluster size was also restricted to $1 \text{ h}^{-1} \text{ Mpc}$. The strength of any observed correlation of the observed galaxy catalog with this matched-filter can be used to measure how well the model matches the data, with the strongest correlations being assigned to cluster candidates. In this way, the PDCS also generated an estimated redshift, a galaxy richness based on the normalization of the luminosity function and other parameters for each cluster candidate based on the best-fitting model. The advantage of this approach has lead other groups to use similar techniques, see for example Dalton et al. (1997), Kepner et al. (1999), Olsen et al. (1999) and Bramel et al. (2000).

Using only the derived quantities from the cluster catalog, the authors of the PDCS found that the space density of clusters of galaxies was 5 ± 2 times that of the space density in the Abell catalog (though the space density is consistent with that found in low redshift automated catalogs such as the Edinburgh-Durham Cluster Catalog and APM cluster catalogs). Secondly, the authors

found no evidence for evolution in the space density with redshift. Both of these results rely on the cluster catalog alone, a catalog based entirely on imaging data.

We have completed a program of obtaining redshifts and velocity dispersions of PDCS clusters to measure the space density as a function of mass as well as richness and X-ray luminosity. This will allow us to both test the original results of the PDCS and possibly provide a complementary sample to that of Carlberg et al. (1997a). We began this program with the X-ray survey of Holden et al. (1997), or H97. Our first spectroscopic observations are described in Holden et al. (1999), H99, but the majority of spectra are from the CFHT Optical PDCS survey which is described in Adami et al. (2000). We summarized our data in §2, with an emphasis on what changes we have made from the previously mentioned papers. We then derive cluster redshifts, velocity dispersions, X-ray luminosities and masses in §3. Using the survey volume estimated in §4, we find the richness and X-ray luminosity function of PDCS clusters in §5. We compute the mass function of PDCS clusters, computed in §6, and find it is consistent with the mass function found for the sample of Carlberg et al. (1997a) given specific choices for the relation between σ_8 and Ω_m , the value of Γ and the form of the richness-mass relation. Finally, in §7 we summarize our results and discuss the future prospects of using optically selected clusters of galaxies to probe theoretical models of cluster formation and evolution. Unless otherwise noted, we use $q_o = 0.1$ ($\Omega_m = 0.2$ and $\Lambda = 0$) and $H_o = 100 h \text{ km s}^{-1}$.

2. Data

Our study comprise of three data sets: the X-ray survey of the PDCS from H97, the spectroscopic sample of H99 and the larger spectroscopic sample of Adami et al. (2000). The spectroscopic survey from H99 contains ~ 100 spectra of galaxies towards sixteen PDCS clusters. The second set of galaxy spectra, the survey described in Adami et al. (2000), contains 636 redshifts towards eleven PDCS clusters. Below, we shall discuss the important details on how each dataset was constructed.

2.1. X-ray Imaging Data

The original X-ray imaging data reduction is discussed in H97. We have repeated the reduction using the new cluster redshifts and in light of the experience of the Bright Serendipitous High-redshift Archival ROSAT Cluster survey (SHARC; Romer et al. (2000)). We shall discuss below the process of image preparation and measuring count-rates for the PDCS cluster candidates with X-ray images. We shall highlight where we used a different approach than in H97.

First we selected PDCS cluster candidates. For a PDCS cluster candidate to be included in our X-ray sample, we required that its optical centroid be less than $40'$ from an X-ray image center. Moreover, the exposure time at the optical centroid had to exceed 3000 seconds in the X-ray image. Thirty-one PDCS cluster candidates met these requirements, see Table 1 for the list of clusters and

H97 for the X-ray data we used.

For each candidate, we derived an aperture for the flux measurement using a “beta” model based on a modified isothermal sphere. We used values for the slope ($\beta = \frac{2}{3}$) and core radius ($r_c = 125 h^{-1}$ kpc) which are typical for rich clusters (Jones & Forman 1992). We converted the above model from physical units to angular units using the estimated redshifts from the PDCS unless a spectroscopic redshift was available. We then convolved the model with empirical model point spread function (PSF) from Nichol et al. (1994). We chose an aperture that contained 80% of the total flux of the PSF convolved model, an increase from the 70% used in H97. We increased the radius based on our experience in the Bright SHARC survey (Romer et al. 2000), where the larger aperture yielded more accurate flux measurement. The resulting aperture radii are listed in column five of Table 1 and range from 2'0 to 5'0 .

Before measuring count-rates, we masked out certain pixels. We masked those pixels that were common to more than one cluster aperture and those pixels that had less than 3000 seconds of exposure. We also ran the source detection algorithm from the Bright SHARC survey on the pointings. We mask any pixels that contained flux from detected sources with centroids more than 1.5' (three times the uncertainty in the PDCS positions) from the PDCS cluster candidates. We note that in two cases, PDCS 36 & 62, we detected a source within 1.5' of the PDCS candidate and we assumed that these detections correspond to those clusters.

After measuring the background subtracted count-rates, we determined which of the thirty-one observations could be classified as detections. For this, we used the (0.4 - 2.0 keV) error map from the ESAS package. The error map is simply the square root of the number of counts in each pixel divided by the exposure time. We converted this back into a map of raw counts. We used the ESAS error map instead of the count-rate map because the ESAS software removes various backgrounds from the count-rate map which are not removed from the error map. In H97 we assumed that a net count-rate that was three times the error estimate represented a three σ (or a 99.87% probable) detection. As the error estimate is derived by the square root of the number of counts in an aperture, this is not correct for a small number of counts. For our new analysis of the X-ray data, we computed the counts in the aperture and the counts expected in the aperture based on the counts in the background annulus. We then computed whether or not a fluctuation in the background could have produce the counts in the aperture. If the counts in the aperture happened less than 0.13% (equivalent to a three σ fluctuation for a Gaussian distribution) of the time by chance, we considered that PDCS cluster to be detected.

Seven PDCS cluster candidates met the detection criterion and they are marked with an asterisk in Table 1, column one. Two of the detections in Table 1 were upper limits in H97. These are now considered detections because of improvements in the source finding algorithm and the increase aperture used to measure fluxes. In Table 1, we list the background subtracted count-rate (column seven). For the 24 PDCS cluster candidates that were not detected, we list an upper limit to their background subtracted count-rate. Our the upper limits are the count-rate that would

produce enough counts to exceed the 99.87% confidence limit.

2.2. Optical Spectra

We have optical spectra from two samples. The first sample was collected with the Kitt Peak Mayall 4m and with the Astrophysical Research Consortium 3.5m telescope. This sample is more fully described in H99. The second set of data were collected using the Canada-France-Hawaii 3.5m Telescope and is described in Adami et al. (2000). The differences between these data sets are in the sample selection and in the number of spectra taken per cluster candidate. Below we will summarize the candidate selection and the data reduction techniques used for both data sets.

2.2.1. KPNO and ARC Data

Thirteen of the sixteen target clusters used in ARC/KPNO spectroscopic survey were selected from the subsample discussed in §2.1. The remaining three (PDCS 11, 12 & 23) were taken from the rest of the PDCS. For details on the spectral extraction and redshift measurement for the ARC/KPNO sample, see H99.

The main goals of the ARC/KPNO survey were to check the measured space density of PDCS clusters and the accuracy of the matched-filter estimated redshifts. Therefore, we selected our targets as independently as possible of the derived parameters given by PDCS. We selected targets using only the net number of $V_4 < 21$, $V_4 - I_4 > 1$ galaxies (the subscript 4 refers to the 4-Shooter camera used to construct the PDCS, see Postman *et al.* 1996 for details on the filter system used and the resulting galaxy catalog) within a 2.5 radius aperture of the PDCS cluster candidates' position. By taking this approach, we still select clusters that potentially have a true redshift vastly different from the PDCS estimated redshift.

2.2.2. CFHT Data

Like the ARC/KPNO sample, the sample of PDCS cluster candidates observed at the CFHT was based on those clusters in the X-ray sample of H97. However, we selected clusters based on their estimated redshifts and their richnesses. We selected clusters differently from the ARC/KPNO for this sample for two reasons. First off, we wanted to create a Richness Class limited sample to compare with the ESO Nearby Abell Cluster sample (Katgert et al. 1996; Mazure et al. 1996). Secondly, in H99, we show that the PDCS estimated redshifts are quite accurate for lower redshift clusters. Therefore, we can select targets using that estimate and be confident that we have a sample of clusters of galaxies that span a limited redshift range.

The selected clusters were all Richness Class 1 or greater ($\Lambda_V > 40$) observed in H97 in either

the $\alpha = 09^{\text{h}}$ or $\alpha = 13^{\text{h}}$ fields. The redshift range was $0.3 \leq z_{\text{estimated}} \leq 0.5$ for both fields. Additionally, one cluster at 00^{h} and one at 16^{h} were observed. All of these clusters observed are listed in Table 2 along with the Λ_V richness and the estimated redshift of the cluster from Postman et al. (1996). PDCS 32, 39 and 45 were not part of our main sample but were observed with masks used for other PDCS clusters.

We used the Multi-Object Spectrograph (MOS) at the CFHT to observe around 50 galaxies per mask in an effort to measure velocity dispersions. For details on the how we constructed multi-object masks as well as how as details on our spectra extraction and redshift measurements for the CFHT sample, see Adami et al. (2000). Briefly, our primary selection consisted of galaxies at or brighter than $M_{\star} = -21.1$ in the V_4 band, no color information was used. We optimally placed the slit-lets using a Minimal Spanning Tree over the $9'.4$ by $8'.4$ MOS field of view. We then filled in the remaining blank spaces of the mask with fainter galaxies. We adjusted our exposure times so that we would successfully measure 70% of the redshifts in our primary sample. Overall, we averaged 66% success for our primary sample, success rates for all of our masks are listed in Table 2 of Adami et al. (2000). We measured our redshifts using cross-correlation (Kurtz & Mink 1998, RVSAO) for 90% of the galaxies. For the remaining 10%, we determined our redshifts using emission lines only.

3. Physical Quantities

Here we discuss how we use the observed redshifts and X-ray count-rates to estimate physically quantities. We begin with how we determined cluster redshifts and velocity dispersions. Using those redshift measurements, we can then compute X-ray luminosities. With the velocity dispersions, we can estimate the binding mass of the clusters of galaxies in our sample.

3.1. Determining cluster redshifts and velocity dispersions

We have two different samples of PDCS cluster candidate redshifts which contain a different number of redshifts. Therefore, we have two different approaches for measuring the redshifts of the PDCS clusters. The large number of redshifts per cluster for some of the CFHT sample also allow us to measure the velocity dispersions. We compare our technique for measuring cluster velocity dispersions with that used by the Canadian Network for Observational Cosmology’s (CNOC) survey of clusters from the EMSS. We then compare our measured redshifts with the estimated redshifts of the PDCS cluster finding algorithm.

3.1.1. ARC/KPNO cluster redshifts

All PDCS cluster candidates in the ARC/KPNO survey had fewer than eight redshifts per cluster, most had only four or five. Therefore, there was only one, if any, peak in the redshift distribution. To estimate the cluster redshift, we computed the median of all the galaxy redshifts for that cluster. If we had three or more concordant cluster members within 1500 km s^{-1} of the median redshift, we considered the candidate to be a cluster of galaxies. We also calculated the mean redshift of all galaxies within 1500 km s^{-1} of the median, in no case did the average redshift change by more than 400 km s^{-1} from the median redshift of the whole sample. The median was a stable estimate of the cluster redshift because, as can be seen in Table 3, most if not all of the galaxies observed were within the 1500 km s^{-1} window on either side of the median (PDCS 02 being the notable exception). If the cluster was not re-observed as part of the CFHT sample, we will use the median cluster redshift, in Table 3, for the rest of this work. See H99 for further discussion on how determined cluster redshifts for the ARC/KPNO sample.

3.1.2. CFHT cluster redshifts and velocity dispersions

In the CFHT sample, we had a much larger number of galaxy redshifts in direction of our PDCS clusters. Simply taking the median of all the available redshifts would not be sufficient for two reasons. First, the large number of intervening field galaxies would eliminate the signal from the cluster and, second, we selected our fields to cover multiple PDCS clusters so there are multiple peaks in the redshift distribution. Instead, we implemented a two step process. The first step is based on the process outlined in Katgert et al. (1996). At each galaxy redshift we searched to see if five or more galaxies were separated by less than 1000 km s^{-1} . For each such over-density, we then found the center and width of the group using the biweight estimators of Beers et al. (1990). The results for the PDCS clusters in our sample are listed in Table 4. The only PDCS cluster not found with this technique was PDCS 34. However, with the addition of the redshifts from the ARC/KPNO survey, PDCS 34 becomes a clear over-density in velocity space.

To assign an over-density in redshift to a PDCS cluster, we calculated the mean Right Ascension and Declination of all of the galaxies within three times the biweight width of the biweight center. Then, we found the PDCS cluster with the closest position. In some cases we had to make large offsets ($\sim 1'$) between the mean position based on the redshifts and the PDCS position. We found this resulted from a galaxy or galaxies far from coordinates the PDCS center but was in the redshift range of the cluster.

Once we found over-densities in the galaxy redshift distribution, each over-density was examined individually. We used a maximum likelihood algorithm to fit a single Gaussian and a flat background to the galaxy redshifts using the technique outlined in Cash (1979). For the range in redshift over which to fit the Gaussian, we chose five times the biweight scale determined above. If the biweight was smaller than the resulting fit, we increased the redshift to include five times

the fitted Gaussian sigma. From the fitted Gaussian, we determine the velocity dispersion of the clusters as well as the mean of the cluster redshifts.

In Table 4, we show our resulting cluster redshifts and velocity dispersions with errors. We plot these fitted Gaussians in Figure 1 on top of our redshift data. We derived the 68% confidence limits in Table 4 using the method outlined in Cash (1979). The error estimates rely on assuming that the likelihood distribution follows a χ^2 distribution. This assumption is true in the case of a large number of data points. For many of our clusters, we do not have a large number of cluster redshifts. This means our error distribution is probably not Gaussian, at least not for large confidence limits (*i.e.* $3 \times \sigma \neq 99.87\%$ confidence limit).

Our maximum likelihood velocity dispersions are smaller than the values derived using the biweight scale from Beers et al. (1990). The median ratio of the biweight scale to the maximum likelihood standard deviation is 1.18 ± 0.17 . Carlberg et al. (1997b) finds a ratio of 1.05 ± 0.04 between the biweight scale and their velocity dispersion estimate, a smaller ratio than ours but not statistically different. Inter-loping field galaxies generally make it much easier to over-estimate than under-estimate the velocity dispersion of a cluster of galaxies, even when using a robust estimator such as the biweight scale. Our maximum likelihood approach explicitly accounts for the background galaxy distribution, so we shall use those estimates for the rest of this work.

Two clusters observed in the CFHT sample, PDCS 45 & 61, are not listed in Table 4 because the Gaussian fitting routine did not converge. For the rest of this work, we will not consider these objects as confirmed clusters of galaxies. However, neither of these two are part of our $\Lambda_V \geq 40$ sample, so our space density estimates are not affected. We would like to note that the total integration time for PDCS 61 was quite low (20 minutes, see Adami et al. (2000)), so it is unlikely we would have detected a cluster of galaxies.

3.1.3. Comparison with the Results from the CNOC survey

To check our technique of estimating velocity dispersions, we measured the velocity dispersions of the eight $z \geq 0.3$ clusters (Ellingson et al. 1997; Abraham et al. 1998; Ellingson et al. 1998; Yee et al. 1998) in the CNOC survey. We can then compare our estimates with those of the CNOC survey.

The CNOC collaboration used a similar approach for determining the cluster velocity dispersions. The authors of the CNOC survey assumed a flat field galaxy background within 15σ of the cluster and used an iterative approach to determine the range in redshift over which to measure the cluster velocity dispersion, see Carlberg et al. (1996). However, the authors used the standard deviation as estimate of the velocity dispersion, instead fitting a Gaussian as we did and the range in redshift used to measure the standard deviation was chosen by visual inspection.

In Figure 2 we show our measurements of the rest-frame velocity dispersion versus those

published by the CNOC survey. Though most of our values agree within two standard deviations, there is one exception in Figure 2. This exception is MS 1512+36, which has a number of peaks in the velocity distribution (Borgani et al. 1999a), see Figure 3. It is likely that the much lower velocity dispersion from the CNOC survey is correct as it agrees with the X-ray luminosity and X-ray temperature of the cluster. This illustrates that our technique works well for most clusters, but not for dynamically complicated ones such as MS 1512+36 because of our explicit assumption of single Gaussian distribution.

Removing MS 1512+36, we find that the average ratio of our dispersion measurements to those from the CNOC survey is 1.05 ± 0.10 . We conclude our technique is equivalent to that of the CNOC for clusters with simple velocity distributions. Therefore, we can compare the distribution of velocity dispersions in our sample with that of the CNOC survey.

3.1.4. Comparison with the Estimated Redshifts in the PDCS

One of the results of the PDCS cluster finding algorithm is an estimated redshift. In Figure 4, we plot the estimated redshift versus our spectroscopically measured redshift as well as the expected 45° line for comparison.

To quantify the observed accuracy of the matched-filter redshifts, we calculated the standard deviation of the difference between the matched-filter redshift and the spectroscopically measured redshift. If we include only those clusters with three or more concordant galaxy redshifts, as discussed above, we estimate the standard deviation to be $\sigma_z = 0.063$ for seventeen clusters with $0.2 \leq z_{est} \leq 0.6$, almost exactly the same as the value we found in H99.

As the scatter in the estimated redshift is important for modeling our cluster selection procedure (see §4.3), we investigated the distribution of the differences between the estimated redshift and the spectroscopic redshift. The average difference between these two redshifts is 0.025, which we find to be not statistically significant from zero according to a Student’s t-test. We also performed a Kolmogorov-Smirnov test to compare the distribution of redshift differences with a Gaussian with a zero mean and a variance as given above. We find no statistically significant difference between our model and the data.

Finally, we checked for any gross change in the distribution with redshift. First we fit a straight line to the data in Figure 4. We then used a χ^2 test and found no statistical difference between the fitted line and a line with a 45° slope and no y-intercept (the line plotted in Figure 4). Second we divide the sample into two equal sized subsamples at $z_{estimated} = 0.4$. Using an F-ratio test, we find no difference between the $z_{estimated} < 0.4$ sample of eight clusters and the $z_{estimated} \geq 0.4$ sample of seven clusters. Therefore, we do not find that the apparent systematic shift in Figure 4 is statistically significant.

For the rest of this work, we will therefore assume the distribution of real redshifts around an

estimated redshift is a Gaussian with a mean of zero and a standard deviation of $0.063_{-0.010}^{+0.012}$ (68% confidence limits from an F-ratio test).

3.2. New X-ray Energy Fluxes and Luminosities

We converted our newly re-measured X-ray count-rates or upper limits to energy fluxes by integrating a redshifted 1.0 keV thermal *bremstrahlung* spectrum over our energy passband of 0.4 - 2.0 keV. We chose 1 keV, as opposed to a 6 keV spectrum as originally used in H97, since it is more representative of clusters in our luminosity range (Reichart et al. 1999a). All fluxes were then corrected for absorption using the observed amount of Galactic neutral hydrogen in the AT&T Bell Laboratories 21 cm survey (Stark et al. 1992) and the cross-section values from Morrison & McCammon (1983). Once we had the energy flux inside the masked aperture (column two of Table 5), we needed to convert to a total flux for each cluster candidate. For cluster apertures where no part of the aperture was masked, the energy flux was simply divided by 0.8 (see previous discussion) to give a total flux (column four of Table 5). For the apertures that were masked, we computed the fraction of the flux from our model that would fall within the masked aperture and then used this fraction to convert between measured and total flux. The total flux (either upper limit or detection) is listed in column three in units of 10^{-14} erg s $^{-1}$ cm $^{-2}$ and the total luminosities are presented in units of 10^{43} erg s $^{-1}$ in are listed in column four of Table 5. For the detections in Table 5, we list errors on the fluxes and luminosities. These errors are the 68% confidence limits for a Poisson distribution using the number of counts in the PDCS cluster candidate aperture. For upper limits, we list the flux and luminosity equivalent to 3σ upper limit for a Poisson distribution.

3.3. Mass Estimates

The simplest way to estimate the mass for a gravitationally bound object in equilibrium is by using the virial theorem. This requires an unbiased estimate of the velocity dispersion, σ and of the size, r_v , of the cluster of galaxies.

It has been shown in a number of papers, see for example in Crone et al. (1994), that the true virialized mass lies within a radius defined by the ratio of the average density inside that radius to the critical density or Δ_c . Inside the radius where this ratio is $\geq 200^6$, objects are found to be virialized while outside this radius the process of accretion is usually still occurring. This motivated Carlberg et al. (1996) to define a mass, M_{200} , based on the mass derived from the virial theorem and combined with an isothermal sphere as a model of the cluster potential. This mass is completely specified by the velocity dispersion (Binney & Tremaine 1987).

⁶It was pointed out to us by Steve Kent that there is a simple derivation for this. The radius for which crossing time for a cluster member equals the Hubble time has a mean interior over-density of ~ 200 .

A modification of the M_{200} comes from Borgani et al. (1999a)

$$M(\sigma_v) = \left(\frac{\sigma_v}{1129 f_{\sigma_v} \text{ km s}^{-1}} \right)^3 \left(\frac{\Delta_c}{178} \right)^{-1/2} E^{-1}(z) 10^{15} h^{-1} M_{\odot} \quad (1)$$

In that paper, they argue that $f_{\sigma_v} = 0.93$ and use $\Delta_c = 178$ for $\Omega_m = 1$ instead of 200 as in Carlberg et al. (1996). The term denoted $E(z)$ is proportional to the time derivative of the logarithm of the scale factor, *i.e.* $H(z) = E(z)^{1/2} H_0$ (Hogg 1999). These masses are $\sim 2/3$ of the M_{200} masses because the different constants used but otherwise directly proportional. For the rest of this work, we will use equation 1 to compute our mass estimates.

3.4. Mass compared to richness

In Figure 5, we plot our masses as measured using equation (1) versus the PDCS V and I band richnesses. We use the mass estimate from equation (1) as that is the closest to mass estimator used in Girardi et al. (1998). We also plot the richness-mass relation from Girardi et al. (1998). To convert between the richness of the PDCS, Λ , and the Abell Richness Class, we use the conversion from Postman et al. (1996) which we list below in Table 7.

The comparison has quite a lot of scatter, even when considering the large errors on our mass estimates. Most of the PDCS clusters appear to match the low-redshift richness-mass relation. However, about $\frac{1}{3}$ of the PDCS clusters fall below the expected line. Many of these are low mass systems which have only a few galaxy redshifts within $3\sigma_v$ of the mean. For example, PDCS 04 is a Richness Class 3 cluster with only five galaxies within $3\sigma_v$ of the mean. Using a simple χ^2 statistic, we tested the idea that our sample contains clusters whose masses were far to low for their richnesses. We find that we can reject at the 99.5% confidence limit the hypothesis that the PDCS mass-richness relation is the same as the Abell mass-richness relation. We find it likely, therefore, that some of the clusters in the PDCS are true over-densities, but have their richnesses over-estimated.

We fit a line to the richness-mass relation of Girardi et al. (1998) which has the following form

$$\log M(10^{14} h^{-1} M_{\odot}) = (1.34 \pm 0.26) \log \Lambda - 1.95 \pm 0.46 \quad (2)$$

and we plot this relation in Figure 5. The fit is rather uncertain because of the small number of data points and the large scatter in mass at each Richness Class. We note here that we fit not the data from Girardi et al. (1998), but instead to the tabulated richness-mass relation. This is equivalent to fitting to the data directly as the Abell Richness estimates are by class. The tabulated values are the solid circles in Figure 5.

4. Survey Volume

An important part of any survey used for statistical purposes is the estimate of the effective survey volume occupied by the objects in the survey. Below we will discuss our modeling of the selection criteria and compute the resulting area and volume coverage for the three surveys.

4.1. X-ray Areal Coverage

Our X-ray data covered parts of three of the five square-degree survey areas in the PDCS. In H97, we calculated the overlap between the PDCS survey areas and the ROSAT pointings to be 1.85 deg^2 . We computed these areas in H97 by finding all pixels with exposure times greater than 3000 seconds and within $40'0$ of the pointing centers. We then found the intersection of these pixels with the part of the sky covered by the PDCS survey fields.

The procedure we used in H97 underestimated the total area covered in the X-ray data. If an X-ray detection lay within $1'5$ of a PDCS cluster candidate position, we considered that detection to be associated with the PDCS cluster candidate. Therefore, we extended the length of the sides of the PDCS survey areas by $1'5$ and recalculated the overlap between the X-ray data and the PDCS survey fields. This procedure yielded an overlap 0.51 deg^2 for the 00^{h} field, 1.14 deg^2 for the 09^{h} field and 0.38 deg^2 for the 13^{h} field. We find, with this improved estimate, that the total area of overlap is 2.03 deg^2 . Our CFHT sample covered 1.52 deg^2 of this area.

4.2. Survey volume for the ARC/KPNO survey

Our ARC/KPNO survey was a sub-sample from the whole of the X-ray cluster candidate sample; *i.e.* 2.03 deg^2 . When determining the survey volume, we must address two issues. First, what is the probability of a cluster at a given redshift to be selected for our ARC/KPNO survey (hereafter $p_s(z)$)? Second, once a cluster is selected, how often would we successfully measure the redshift of that cluster given our observing strategy ($p_r(z)$)? These two probabilities are then included in the following equation

$$V = \int_{z_1}^{z_2} \frac{dV}{dz} p_s(z) p_r(z) dz \quad (3)$$

where $\frac{dV}{dz}$ is determined by q_o , H_o and the survey area while the two probabilities, $p_s(z)$ and $p_r(z)$ are determined by our selection criteria, the underlying cosmological parameters and our observing strategy. We performed Monte Carlo simulations of both our selection procedure and our observing strategy to answer these questions. The details of these simulations are found in H99 but below we will review the salient points.

To compute the probability of a cluster being selected for our survey, $p_s(z)$, we constructed

model PDCS clusters and simulated the selection process outlined in §2.2.1. We created model clusters using a power-law profile (Lubin 1996) and a Schechter luminosity function from Colless (1989) to represent the distribution of positions and luminosities for the galaxies in the cluster. For each simulated cluster, we used random values for the parameters based on the ranges specified in Lubin (1996) and Colless (1989). The normalization of the luminosity function was a randomly chosen richness from the values in the PDCS catalog. The resulting probabilities from these simulations are illustrated, as a function of richness and redshift, in Figure 4 of H99.

To model our redshift completeness, which determines $p_r(z)$ in equation (3), we created artificial redshift distributions using a Gaussian to represent the cluster velocity distribution and the Canada-France Redshift Survey to represent the background galaxy redshift distribution. We used the same parameters and observational limits as in H99 for determining the number of cluster members inside the Gaussian velocity distribution. Our simulation results can be seen in Figure 6 where we plot the probability of successfully measuring the redshift of a cluster in our ARC/KPNO sample.

To perform the integral in equation (3), we must set the bounds of the integral. We chose $z_1 = 0.1$ as that is the lower redshift limit of the PDCS. For z_2 , we computed where $p_r(z)$ dropped below 5% which yields $z_2 = 0.55$ for Richness Classes 1 and 2 and $z_2 = 0.57$ for Richness Class 3. These numbers are higher than those found in H99, because for that work we were limited by a small number of redshift per cluster. The addition of the redshifts from the CFHT survey of the clusters in common with the ARC/KPNO survey allow us to extend the redshift range of the ARC/KPNO sample. By extending the redshift range, we survey a larger volume than in H99 and include more PDCS clusters.

For both sets of simulations, the important independent variables were redshift and Richness Class. The authors of the original PDCS survey provide no results for Richness Class 0 clusters, so though we can calculate a volume for those clusters, we will not consider those clusters for statistical tests. When we combine the results of both sets of simulations, we found we surveyed $15.7 \times 10^4 \text{ h}^{-3} \text{ Mpc}^3$ for the Richness Class 1 clusters and $20.4 \times 10^4 \text{ h}^{-3} \text{ Mpc}^3$ for the Richness Class 2 clusters.

We investigated the change in enclosed volume as a function of the various model parameters. We assumed for all of these tests that $p_r(z) = 1$, so we did not have to run two sets of simulations. In Table 6, we show how changing various parameters changes the volume surveyed for Richness Class 2 clusters. The most surprising result is that by changing the absolute magnitude of M_\star by -0.1 magnitudes, an increase in the luminosity, the change in the enclosed volume is only +0.2% while a increase of 0.1 magnitudes decreases the volume by 10%. This small change in volume for an increase in M_\star stems from the steeply increasing K corrections. In the redshift range of $0.3 \leq z \leq 0.4$, the 4000 Å break moves through the V filter causing the K corrections to increase rapidly. For example, from $z=0.36$ to $z=0.40$, the K correction changes by 0.2 magnitudes. Therefore, an increase in M_\star does not increase the effective limiting redshift of the sample.

As a check of the K corrections, we tried the elliptical galaxy K corrections, without the additional evolutionary corrections, of Poggianti (1997), which we find changes the enclosed volume by -10%. We can conclude, using the results of Table 6, that the uncertainty in our survey volume from systematic shifts in the individual model parameters is on the order of $\sim 10\%$.

4.3. Survey volume for the CFHT survey

The PDCS cluster candidates in the CFHT survey were selected to be within the estimated redshift range $0.3 \leq z_{estimated} \leq 0.5$ and have V-band richness $\Lambda_V \geq 40$ from the PDCS catalog in Postman et al. (1996). We chose candidates for our sample from the 09^h and 13^h fields as covered by the X-ray survey from H97. We observed all candidates that met our criteria but PDCS 36. The area we covered is 1.52 deg² with the majority of that area in the 09^h field.

To compute the volume we surveyed, we need to compute $p_s(z)$ and $p_r(z)$ for equation (3), as we did for the ARC/KPNO sample. Instead of using Monte Carlo simulations as above, we chose an analytical model for $p_s(z)$ and $p_r(z)$. We selected our clusters for the CFHT sample based completely on the results of the PDCS so to perform Monte Carlo simulations correctly would require simulating the PDCS selection process. Instead, we rely on the simulations done by the authors of the PDCS catalog. These simulations show that, assuming the same elliptical galaxy type K corrections as we use in §4.2, the PDCS has a 100% probability of successfully detecting a Richness Class 1 $z = 0.4$ in the V band, with a 100% probability of detection at $z = 0.55$ for Richness Class 2 or greater.

The analytical model for our probability of selection was

$$p_s(z_{est}|z) = \int_{z_{est}-\delta_z}^{z_{est}+\delta_z} \frac{1}{\sqrt{2\pi}\sigma_z} \exp \frac{-(z - z_{est})^2}{2\sigma_z^2} dz \quad (4)$$

where z_{est} is the estimated redshift from the PDCS catalog, z is the actual redshift of a clusters, $\delta_z = 0.05$, or half the interval between PDCS estimates redshifts. The scatter in the Gaussian, $\sigma_z = 0.063$, was determined in §3.1.4 (see Figure 4). We can invert the above equation to predict $p(z|z_{est})$ if we make the assumption that all values of z and z_{est} are equally likely. We then multiply the probability above with the simulation results from the PDCS. The product of these two probabilities determines $p(z)$ in equation (3) for the estimated redshift range in our sample.

The remaining quantities to be determined are the limits on the integral in equation (3) and the probability of successfully measuring the redshift a cluster, $p_r(z)$. We assume because of the large number of spectra we collected per cluster candidate (≥ 40) that $p_r(z) = 1.0$ for our $\Lambda_V \geq 40$ and $0.3 \leq z \leq 0.5$ PDCS sample. The main limit on the redshift range is the sensitivity of our spectrograph and the blocking filters we used. The two blocking filters we used spanned from 0.20-0.56 and 0.43-0.61 in redshift. Therefore, we chose $z_1 = 0.2$ and $z_2 = 0.61$. Therefore, the resulting volume is $31.7_{-0.8}^{+0.5} \times 10^4 \text{ h}^{-3} \text{ Mpc}^3$ for Richness Class 2 and greater clusters and $21.9_{-0.8}^{+0.5} \times 10^4 \text{ h}^{-3} \text{ Mpc}^3$ for Richness Class 1 clusters.

The main uncertainty in the above estimate of the survey volume is the actual shape of the $z_{estimated} - z$ probability distribution, which we assumed to be Gaussian. In §3.1.4 we test our assumption the distribution is a Gaussian and that the mean of the distribution is zero. Nonetheless, as an alternative, we used the actual distribution of redshift differences to compute a volume of $24.7 \times 10^4 \text{ h}^{-3} \text{ Mpc}^3$ for Richness Class 2 or greater clusters. Therefore, we conclude our error on the survey volume is, at most, $\sim 20\%$.

5. X-ray and Richness Space Density

The combination of the ARC/KPNO sample and the CFHT sample will allow us to measure the space density of PDCS clusters as a function of a number of independent variables. Here we will discuss the density of PDCS clusters as a function of richness and X-ray luminosity, leaving the mass for §6.

5.1. Space Density as a Function of Richness

The original PDCS catalog paper (Postman et al. 1996) used the estimated redshifts and richnesses to compute the space density of clusters as a function of richness. The authors of the PDCS found that the space density for the PDCS was about five times that of the Abell catalog for a given Richness Class and did not evolve with redshift. The original purpose behind the ARC/KPNO sample was to check this result. In H99, we found our survey to be in agreement with Postman et al. (1996). Here we will improve on that work using our larger sample of PDCS clusters.

To compute the space densities, we group the clusters by Richness Class using the conversion between Λ and Richness from Postman et al. (1996) (see Table 7 for the conversion). We used both the V and I band Λ values separately. We then divided the number of clusters in each class by the volumes from §4.2 and §4.3. The resulting number of clusters in each class and densities are listed in Table 7, with the ARC/KPNO sample and the CFHT sample listed separately.

We plot the Λ_V densities from Table 7 in Figure 7 in comparison with those from Postman et al. (1996). We find a good match between the space density of clusters in our sample and in the original PDCS. This is not surprising given how good the estimated redshifts are in the PDCS. The only way we would have found a serious discrepancy is if a large number of PDCS clusters turned out to be false positive detections, which is not the case.

We compare our data with a sample of low redshift clusters of galaxies created using the same algorithm, the sample of Bramel et al. (2000). This sample, also known as the Edinburgh-Durham Cluster Catalog 2 (EDCC2), used the algorithm of the PDCS to find clusters of galaxies in the Edinburgh-Durham Galaxy Catalog. We re-scaled the densities from Bramel et al. (2000) to those

appropriate for a $q_o = 0.1$ cosmology and plot the resulting densities in Figure 7 as open triangles.

In Figure 7, we also plot the space density of clusters of galaxies from the APM cluster catalog (Dalton et al. 1997) using the densities from Croft et al. (1999). The APM catalog is a low redshift ($z \leq 0.1$) catalog constructed using a related but somewhat different technique than the PDCS. We converted between the APM richness and the Λ richness using the values Table 1 and 2 of Dalton et al. (1997) for the sample used in Croft et al. (1999).

As demonstrated in Figure 7, our space density measurements for the PDCS are in good agreement with those from three different analyses; EDCC2, APM and the original PDCS. Given this strong agreement between the high redshift measurements from the PDCS and the results of the low redshift catalogs, we have confirmed the claim in Postman et al. (1996) for no apparent evolution in the richness function out to $z = 0.5$.

5.2. Space Density as a Function of X-ray Luminosity

Using the volume estimates from §4, we can compute the space density of clusters as a function of X-ray luminosity. The main concern here is that most of the PDCS clusters are not X-ray detections but are upper limits. Secondly, our sample is quite small compared with X-ray selected cluster surveys. Therefore, our X-ray luminosity function is a check of the PDCS. In other words, does it contain all the clusters it should contain or does it miss clusters an X-ray selected sample would find?

We plot, in Figure 8, the cumulative number of detections using solid circles. We also plot, with open circles, the cumulative distribution of upper limits and detections. To construct this cumulative distribution, we used a Kaplan-Meier product limit estimator (Feigelson & Nelson 1985; Schmitt 1985). This is a parameter free estimator that allows us to use both the upper limits and the detections. We use the formulation from Schmitt (1985) which is tailored for luminosity functions.

$$N(L_x > L_{x,i}) = 1 - \prod_{i, L_{x,i} > L_x}^n \left(1 - \frac{d_i}{n_i}\right) \quad (5)$$

where L_x is the X-ray luminosity, $L_{x,i}$ is the X-ray luminosity of the i^{th} cluster, n_i is the number of clusters with $L_{x,i} \leq L_x$ and d_i is the number of clusters with $L_{x,i} = L_x$ so is either 1 or 0 for our sample. As pointed out in Briel & Henry (1993), this technique assumes that we know precisely the values of the upper limits or of the detections. Even our detections are at a low ($\sim 3\sigma$) significance while there is a small probability that a upper limit could be smaller than the actual cluster luminosity. Thus, this is a significant source of error.

We also plot, using squares, the cumulative distribution function for the ARC/KPNO sample. Once again we plot both using only the detections (solid squares) and both the detections and the upper limits (open squares). The luminosity function for the ARC/KPNO survey is higher than

that for the CFHT survey and higher than the other published samples. A likely explanation for this is we under-estimated the volume surveyed for the ARC/KPNO sample.

For comparison, we plot in Figure 8 the cumulative X-ray luminosity functions from two low redshift samples: Burns et al. (1996) (solid line) and the power law component of the Schechter luminosity function from Ebeling et al. (1997) (dotted line). We also plot power-law fits Burke et al. (1997) (dot-dashed) and Rosati et al. (1998) (+ symbols), two samples of the same redshift as our PDCS sample. All the lines are for $h = 0.5$ and $q_o = 0.5$, so we recomputed our survey volume and X-ray luminosities for these values.

There are two moderate to high redshift samples of optically selected clusters of galaxies with X-ray luminosity functions. One sample, Castander et al. (1994), has a lower space density at roughly the same luminosities as our sample. However, the sample of Castander et al. (1994) is at much higher redshift than our sample, so the disagreement with our luminosity function could be explained by evolution. The second sample is from Bower et al. (1994). In that sample, almost all of the clusters of galaxies are detected, but the luminosity function was estimated using both the detections and upper limits. That sample shows a decrease in the luminosity function as well, though the mean redshift $\bar{z} = 0.42$, quite close to our mean redshift $\bar{z} = 0.38$. The more recent X-ray selected samples of clusters of galaxies cast doubt on the results of Bower et al. (1994), as surveys such as Burke et al. (1997) and Nichol et al. (1999) find no evidence for evolution in the same range of luminosities and redshifts.

Nonetheless, we confirm in Figure 8 that the space density of PDCS clusters is higher compared to X-ray selected samples of clusters of galaxies. Most of these clusters of galaxies, however, are not detected as X-ray emitters. This differs from other X-ray surveys of optically selected clusters (Briel & Henry 1993; Castander et al. 1994; Bower et al. 1994; Burg et al. 1994) which find that 50% or more of the clusters in those samples are detected. When using only the detections in our sample, we find a cumulative distribution that matches X-ray selected surveys for the CFHT sample. Therefore, it appears that the PDCS did not miss clusters that an X-ray selected survey would find.

6. Space Density as a Function of Mass

We measured velocity dispersions of PDCS clusters of galaxies to compare the resulting distributions with low redshift samples and as a complement to other high redshift samples, such as the CNOC cluster survey mentioned earlier.

In Figure 9 we plot the cumulative distribution of cluster masses in our sample. We also plot the error bars on the mass measurements. The errors bars on the number density are comparable to those found in our X-ray luminosity function in Figure 8. We also plot, on this diagram, the mass function of the CNOC cluster survey using the velocity dispersions published in Carlberg et al. (1996). We note here that we plot the entirety of our sample, we do not try to create a subsample

that is complete to some limiting velocity dispersion as is done in Carlberg et al. (1997a) and Borgani et al. (1999a). However, we plot the X-ray luminosity and velocity dispersion limited sample from Carlberg et al. (1997a). Though the two cumulative distributions do not overlap, we see we fulfilled our goal of creating a complementary survey to the CNOC survey. Most of clusters are at a smaller mass than those found in the CNOC survey. The combination of the two surveys now covers over three orders of magnitude in space density.

The main problem with using our sample for measuring the mass function of clusters of galaxies is the quality of our mass measurements. As we show above, the mass depends on the velocity dispersion cubed (see equation 1), and most of our velocity dispersion measurements have errors up to $\sim 50\%$, yielding errors on the mass of $\sim 150\%$. The question becomes how to take advantage of our data, an almost complete subsample of the PDCS with velocity dispersions, while minimizing the impact of our errors.

We elected to approach this problem by finding the best fitting theoretical mass function. We can then compare this best fit with the results from other samples with much smaller errors. In Figure 9, we plot three curves. These are best fitting theoretical mass functions to different data sets, generated using the model discussed below. The solid line is from the results of Bahcall et al. (1997), the dashed line is based on a fit to the mass function of the CNOC survey by Carlberg et al. (1997a) and the dotted line is our fit to the mass function of our data. All three theoretical curves are the result of letting two parameters Ω_m , the mass density of the universe, and σ_8 , the normalization of the power spectrum of mass fluctuations vary. Each combination of these two parameters predicts a different mass function, which is then compared with the data to find a best fitting model.

Our theoretically expected mass functions are based on the semi-analytical model originally from Press & Schechter (1974). We specifically used the formalism outlined in Viana & Liddle (1996). Thus, we used the following to model the density fluctuations spectrum

$$\sigma(R) = \sigma_8 \left(\frac{R}{8h^{-1}\text{Mpc}} \right)^{\gamma(R)} \quad (6)$$

where $\gamma(R)$ depends on Γ and a few constants. The scale R is related to the mass M by the density $M = 4\pi R^3 \rho$. The form of $\gamma(R)$ is based on a fit to the spectrum of fluctuations in cosmic microwave background and in the distribution of galaxies. The term σ_8 in equation (6) has a redshift dependence that is different for different values of Ω_m . To account for this dependence, we use the equations from Viana & Liddle (1996).

As we fixed $\Gamma = 0.23$ in equation (6), we have two free parameters: Ω_m and σ_8 , two of the parameters that we said earlier are the most important for determining the number density of virialized masses. We could vary these independently, but instead we chose to use the relation $\sigma_8 = 0.60\Omega_m^{-0.48+0.17\Omega_m}$ from Girardi et al. (1998). This particular relation was the result of a fit to a low redshift sample of clusters of galaxies which makes comparing with the results of Girardi et al. (1998) easier. As this relation results from a fit, instead of an analytical derivation, there is

an error associated with the fitted parameters on the order of $\sim 10\%$. Other papers (Bahcall et al. 1997; Borgani et al. 1999a) have found a similar relation with as the above but with constants that vary on the order of $10\% - 20\%$ from the numbers above.

The Press-Schechter formalism predicts the space density of clusters of galaxies as a function mass. However, what we measured were the velocity dispersions of clusters. To convert the masses into velocity dispersions, we used the estimate of Borgani et al. (1999a), or equation (1). This allows us to fit our distribution of observed velocity dispersions as a function of the above parameters using the Press-Schechter formalism.

To estimate which value of Ω_m best agrees with our velocity dispersion measurements, we used a maximum likelihood estimator. In particular, we used the approach of Cash (1979) and Marshall et al. (1983), where we compute

$$S = -2 \ln L = -2 \sum_{i=1}^N \ln \left[\frac{dN(z_i, \sigma_{v,i} | \Omega_m, \sigma_8)}{dM} \frac{dV(\Lambda_i | \Omega_m, \sigma_8)}{dz} \right] - E(\Omega_m, \sigma_8) \quad (7)$$

z_i is the observed redshift a cluster, $\sigma_{v,i}$ is the observed velocity dispersion of a cluster, Λ_i is the observed richness, N is the total number of observed clusters in the sample, and E is the expected total number of clusters in the sample, a double integral of the model over the redshift and mass range of the sample. We note here that for every different value of Ω_m , we recomputed the survey volume using the prescription in §4.3.

To compute E in equation (7) requires that we have a relation between the mass and the richness. We used the richness-mass relation in equation (2). We will assume that the richness-mass relation does not evolve with redshift as we do not have data in our sample to test for such evolution. We note here, however, that this is one of the most likely sources of systematic error in addition to the large statistical error in the relation (see Figure 5).

To included the errors in our velocity dispersion measurements, we convolved the $\frac{dV}{dz} \frac{dn}{dM}$ term in equation (7) with a Gaussian of the width of the errors in the velocity dispersion when computing the likelihood for a cluster given a specific model. The process is outlined in Burke et al. (1997) and Nichol et al. (1997) and is similar to the process in Borgani et al. (1999a).

Using equation (7), we computed the likelihood for various values of Ω_m . We found the best fit to be $\Omega_m = 0.32 \pm 0.08$ (68% confidence limits for 1 parameter). The small apparent error on our estimate can be deceiving as it is a result of the relation $\sigma_8 = 0.60\Omega_m^{-0.48+0.17\Omega_m}$. Most of the clusters in our sample have masses at the value of the mass enclosed in a $8 h^{-1}$ Mpc sphere so our fit to the mass function is most sensitive to σ_8 , the normalization of the power spectrum in equation 6. This also means that our results are insensitive to changes in the parameters the change the shape of of the mass function, such as Γ and Ω_m . Therefore, when we force a specific relation between Ω_m and σ_8 , it appears we constrain Ω_m well, however the only parameter we really can attempt to constrain is σ_8 . If instead imposing the relation between Ω_m and σ_8 , we allow Ω_m and σ_8 to be independent, our 68% confidence limits for Ω_m span $0.1 \leq \Omega_m \leq 1.0$.

We plot in Figure 9 the cumulative mass function based on the best fitting value of Ω_m to our data as the dotted line. One important thing to note is that the mass function has a redshift dependence. We plot the theoretical mass functions for $z = 0.4$ but our data and the CNOC data cover a redshift range of $0.2 \leq z \leq 0.6$. Nonetheless, the dotted line, our best fit, agrees well with our data and the CNOC cluster masses.

For comparison, the authors of Carlberg et al. (1997a) found a best fitting $\Omega_m = 0.4$ and a best fitting $\sigma_8 = 0.75$ using the CNOC cluster survey. Bahcall et al. (1997), which used the PDCS in part, found a best fitting $\Omega_m = 0.2$ and $\sigma_8 = 0.85$. These values are only for comparison, each of them uses a different value of Γ as well as different relations between σ_8 and Ω_m . In fact, in the re-analysis of Carlberg et al. (1997a), Borgani et al. (1999a) finds a range of allowed values of Ω_m depending on the relation between σ_8 and Ω_m used. However, Borgani et al. (1999a) did find the best range to be $0.35 \leq \Omega_m \leq 1.0$. The important result is that our results are in agreement with the results of Carlberg et al. (1997a) and Borgani et al. (1999a) when we make similar specific assumptions for the value of Γ and for the relation between σ_8 and Ω_m .

When we vary the relations we used, we greatly increase our uncertainty. For example, if we shift the scale of the richness-mass relation (equation 2) by half a richness class, the best fitting values range $0.26 \leq \Omega_m \leq 0.34$. In the simulations of the PDCS algorithm, it was found that some PDCS clusters could be shifted as far as a whole Richness Class, which would cause an even larger shift in the best fitting value of Ω_m . Furthermore, the large scatter in the observed richness-mass relation means we have a number of low mass clusters contaminating our sample.

7. Discussion and Conclusions

In this paper we presented redshift measurements, velocity dispersions and X-ray imaging data for a subset of the PDCS. We aimed to construct the first dataset of velocity dispersions of a subsample of the PDCS. This dataset was constructed to be complementary to the CNOC cluster survey and to be easily compared with lower redshift samples. Our goal was to use this dataset to determine the space density of clusters of galaxies in the PDCS catalog as a function of richness, X-ray luminosity, and mass. We could then compare these space densities with low redshift samples to test the apparent lack of evolution in the PDCS cluster catalog and to compare the distribution of masses with the expectations of cluster formation theory.

We began this process by collecting X-ray imaging data for a total of thirty-one cluster candidates in the PDCS. We followed up the X-ray imaging data with spectroscopy of PDCS cluster candidate galaxies. We successfully measured redshifts for seventeen PDCS clusters (fifteen of which we have X-ray imaging data for). The PDCS clusters of galaxies for which we have redshifts are part of two samples with different selection criteria. One sample, the ARC/KPNO sample, was selected on the number of $V - I \geq 1$, $V \leq 21$ galaxies in a $2.5'$ circle centered on the PDCS cluster candidate position. This provided a sample selected independently of many of the derived

cluster parameters in the PDCS (such as richness, estimated redshift, *etc.*) Our second sample, the CFHT sample, was selected using cluster parameters from the catalog, specifically all clusters in the X-ray imaging data with $\Lambda_V \geq 40$ and $0.3 \leq z_{estimated} \leq 0.5$ where Λ_V is the richness estimate of the PDCS in the V filter. This second sample was constructed to mimic the selection of the ESO Nearby Abell Cluster Survey in that we selected clusters of Richness Class 1 or greater (Katgert et al. 1996).

Given these two samples of redshifts, we then derived redshifts for the clusters, and, when possible, velocity dispersions based on the galaxy redshifts. We fit a Gaussian plus flat background using a maximum likelihood estimator to measure the velocity dispersions. This approach has the advantage of using the galaxy velocities directly and is completely automated. However, as we made an explicit choice on the shape of the velocity distribution, we are biased towards over-estimating the velocity dispersion of clusters with complicated dynamics. We tested our approach using the published CNOC velocities and found that for seven out of the eight clusters we measured the same velocity dispersions and the same size errors, $\sim 10\%$. The one exception was MS 1512+36, a dynamically complicated cluster with two secondary peaks in the velocity distribution. Most of the clusters in our sample had a much smaller number of cluster members than the CNOC sample. Therefore, our velocity dispersions had much larger errors, up to $\sim 50\%$.

Using the redshifts, we measured X-ray luminosities or upper limits for thirty-one PDCS cluster candidates. We chose to measure our X-ray luminosities within an aperture that contains a fixed fraction of the total flux, using a β model to calculate the size of that aperture. For those sixteen PDCS cluster candidates for which we did not have spectroscopic redshifts, we used the estimated redshifts of the PDCS to compute the apertures. Twenty-four of the candidates in our sample were not X-ray detections. For those, we assigned 3σ upper limits on the flux and luminosity.

When we compare our masses derived from the velocity dispersions to the richnesses in the PDCS catalog in Figure 5, we find that $\frac{1}{3}$ of our masses are lower than the expected values based on the richnesses. For example, we have in our sample two Richness Class 3 clusters with velocity dispersions of only $\sim 500 \text{ km s}^{-1}$, with implied masses around $1 - 3 \times 10^{14} h^{-1} M_\odot$. We find that the relation between masses and richnesses in the PDCS sample differs from the Abell mass-richness relation from Girardi et al. (1998) at the 99.5% confidence limit. This observed difference comes from these low mass systems with high richnesses.

In §4.2 and 4.3 we derived the volumes surveyed for our two samples. We find that these volumes are accurate to around $\sim 20\%$ except for changes in q_o . These are much smaller errors than our errors based on our sample size. We used these volumes to derive the space density of PDCS clusters as a function of richness, X-ray luminosity and mass. If we examine the richness function of the clusters in our sample, we find space densities in line with those of the whole of the PDCS. As we mentioned before, this result is not surprising given how accurate the estimated redshifts are for the clusters in our sample and that most of the candidates in the PDCS are true over-densities of galaxies. Based on this result, we find that the PDCS agrees with the space

densities for lower redshift catalogs of clusters of galaxies like the EDCC2 of Bramel et al. (2000) and the APM results from Croft et al. (1999). However, this raises the question of why all of these catalogs find a much higher space density of clusters of galaxies than the Abell catalog at ostensibly the same richnesses?

To try to answer this question, we first look at a different distribution function, the X-ray luminosity function. What is interesting is that the X-ray luminosity function of PDCS clusters of galaxies is quite in line with those based on X-ray selected samples, such as Burke et al. (1997) and Rosati et al. (1998) as well as those based on other optically selected samples such as Burns et al. (1996). This means that it is unlikely that the PDCS missed any X-ray emitting clusters of galaxies. However, considering that most of the clusters of galaxies are not detected in our X-ray data, those clusters must have quite faint luminosities ($\leq 10^{43}$ erg s $^{-1}$, see Figure 8). The clusters at those luminosities in the optically-selected, low redshift sample of Burns et al. (1996) are quite poor, being either Richness Class 0 Abell clusters or groups from the catalog of White et al. (1999).

If we examine the mass function, once again we find that the distribution of masses in our sample matches that of other samples. We chose to compare our mass function with those of other samples by finding which cosmological parameters are most likely to produce the distribution of masses in our sample. We find the best fitting Ω_m to be quite in line with those from the CNOC cluster survey if we assume both the $\sigma_8 - \Omega_m$ relation and the richness-mass relation from Girardi et al. (1998). By the theoretical mass function that best fits our data, we see that most of our clusters should have masses on the order of $\sim 10^{14}$ h $^{-1}$ M $_{\odot}$, which is in agreement with our data, and is the mass range found for Richness Class 0 and 1 clusters in Figure 5.

Based on our data, we find that the PDCS finds clusters of galaxies have distributions of mass and X-ray luminosity that match those of other samples. This leaves the richness function as the discrepant function, but only when compared with the Abell catalog. Other optically selected catalogs of clusters of galaxies find a much higher space density of objects than the Abell catalog, such as the APM cluster catalog (Dalton et al. 1997) or the Edinburgh-Durham Cluster Catalog 2 (Bramel et al. 2000). Therefore, it is likely that either the Abell catalog is strongly incomplete by a factor of three or four, a rather unlikely occurrence, or that there is a mismatch between the various richness measures used by the automated catalogs and the Abell Richness. These ideas will be tested with future cluster catalogs that cover a large area of the sky, such as the DPOSS (Gal et al. 2000) and SDSS cluster catalogs.

The promise of optically selected catalogs has always been that, given the relative ease of collecting large amounts of imaging data, catalogs with literally thousands of clusters of galaxies could be constructed. Our investigations of the PDCS shows that modern sophisticated cluster finding algorithms do an excellent job of finding over-densities of galaxies and correctly estimating their apparent redshift. From Figure 9, we can see that it will be possible to use optically selected clusters of galaxies to study cluster formation and evolution. The challenge will lie in improving the contrast for truly massive systems, to decrease the contamination we see in Figure 5. Machine based

richnesses appear to be only an incremental improvement over counts by eye (Victoria Alonso et al. 1999, for a comparison of richness to mass for the APM and Abell catalogs). A possible solution could be in using such techniques as a color-based or photometric redshift selection, see for example Kepner et al. (1999) or Gal et al. (2000). The approaches have the promise of reducing the number of contaminating field galaxies in cluster candidates. A second solution would be to replace a simple count of the number of galaxies with new measures of the total galaxy content such as the total luminosity from Adami et al. (1998), Fritsch & Bheuhert (1999) or Miller et al. (2000). Catalogs using the combination of these two techniques should have the observed optical galaxy signal much more strongly correlated with mass. With such improvements and the new large area surveys such as the SDSS and DPOSS, optically selected clusters can be used to probe the mass function over 4 or 5 orders of magnitude in density and, thus, be used to explore the formation of the most massive gravitationally bound objects observed.

This paper represents the submitted version of BH's dissertation. I would like to thank a number of people for reading over various versions of this work. This list includes Rich Kron, who read the whole thing at least twice, and my collaborators: Christophe Adami, Francisco Javier Castander, Lori Lubin, Robert Nichol, and A. Katherine Romer. I would also like to thank the anonymous referee for improving this paper. For help in understanding statistics, I thank Erik Reese for many useful pointers and Carlo Graziani who spent hours explaining Maximum Likelihood parameter estimation and the theory behind confidence limits. I would like to credit Gil Holder for correcting many of my misunderstandings of the Press-Schechter formulation and for testing my predictions of the cluster mass function. Daniel Reichart also helped with my understanding of Press-Schechter theory as well as all of the pitfalls of converting observational quantities like richness into the masses predicted from theory. Finally, I would like to thank Chris Metzler and Martin White for long explanations during the Cluster Eating Group about cluster formation and the spherical collapse model, I would like to thank Chris especially for his long patient explanations of relating theoretical predictions to observations.

For scientific guidance, I would like to thank Rich Kron for teaching so well his particular way of looking at observational data. His intuition and ability to quickly get to the heart of a complicated collection of numbers served me well, despite my writing a thesis in a field that is not his specialty. I owe a great debt to Bob Nichol for teaching me, on a daily basis, how to start, progress, and complete a scientific project. Without his ideas and guidance, I would have been a graduate student much longer. I only hope I can learn how to form the ideas that he does. Kath Romer has taught me almost all of the X-ray astronomy I know, and good deal of the optical astronomy as well. She also patiently waded through the horrid language of my first paper, molding it into something that could be read and understood. Francisco Castander had many long conversations with me about cluster X-ray emission, stellar population synthesis, and all sorts of other fields of astronomy. I would like to thank Lori Lubin taking the time to repeatedly dig through all of her old notes to answer my obscure questions about the PDCS. I would also like to thank her for providing very insightful comments on earlier drafts of this dissertation and my other papers. In addition, I would

like to thank Mel Ulmer for scientific and financial support all throughout my graduate career, as well as a fresh perspective on many different scientific problems.

This project was funded in part by NASA grant NAG5-3202. BH was partially supported by the Center for Astrophysical Research in Antarctica, a National Science Foundation Science and Technology Center, by NASA GO-06838.01-95A and by NSF AST-9256606. This research was supported through NASA ADP grant NAG5-2432 (at Northwestern University) and NASA LTSA grant NAG5-6548 (at Carnegie Mellon University).

REFERENCES

- Abraham, R. G., Yee, H. K. C., Ellingson, E., Carlberg, R. G., & Gravel, P. 1998, *ApJS*, 116, 231
- Adami, C., Holden, B. P., Castander, F. J., Nichol, R. C., Mazure, A., Ulmer, M. P., Postman, M., & Lubin, L. M. 2000, *AJ*, submitted
- Adami, C., Mazure, A., Biviano, A., Katgert, P., & Rhee, G. 1998, *A&A*, 331, 493
- Bahcall, N., Fan, X., & Cen, R. 1997, *ApJ*, 485, 53
- Beers, T. C., Flynn, K., & Gebhardt, K. 1990, *AJ*, 100, 32
- Binney, J. & Tremaine, S. 1987, *Galactic Dynamics* (Princeton: Princeton University Press)
- Borgani, S., Girardi, M., Carlberg, R. G., Yee, H. K. C., & Ellingson, E. 1999a, *ApJ*, 527, 561
- Borgani, S., Rosati, P., Tozzi, P., & Norman, C. 1999b, *ApJ*, 517, 40
- Bower, R. G., Böhringer, H., Briel, U. G., Ellis, R. S., Castander, F. J., & Carter, D. 1994, *MNRAS*, 268, 345
- Bramel, D., Nichol, R. C., & Pope, A. 2000, *AJ*, submitted
- Briel, U. G. & Henry, J. P. 1993, *A&A*, 278, 379
- Burg, R., Giacconi, R., Forman, W., & Jones, C. 1994, *ApJ*, 422, 37
- Burke, D. J., Collins, C. A., Sharples, R. M., Romer, A. K., Holden, B. P., & Nichol, R. C. 1997, *ApJ*, 488, L83
- Burns, J. O., Ledlow, M. J., Loken, C., Klypin, A., Voges, W., Bryan, G. L., Norman, M. L., & White, R. A. 1996, *ApJ*, 467, L49
- Carlberg, R. G., Morris, S., Yee, H. K. C., & Ellingson, E. 1997a, *ApJ*, 479, L19
- Carlberg, R. G., Yee, H. K. C., & Ellingson, E. 1997b, *ApJ*, 478, 462
- Carlberg, R. G., Yee, H. K. C., Ellingson, E., Abraham, R., Gravel, P., Morris, S., & Pritchett, C. J. 1996, *ApJ*, 462, 32
- Cash, W. 1979, *ApJ*, 228, 939
- Castander, F. J., Ellis, R. S., Frenk, C. S., Dressler, A., & Gunn, J. E. 1994, *ApJ*, 424, L79
- Colless, M. 1989, *MNRAS*, 237, 799
- Croft, R. A. C., Dalton, G. B., & Efstathiou, G. 1999, *MNRAS*, 305, 547
- Crone, M. M., Evrard, A. E., & Richstone, D. O. 1994, *ApJ*, 434, 402

- Dalton, G. B., Maddox, S. J., Sutherland, W. J., & Efstathiou, G. 1997, *MNRAS*, 289, 263
- Ebeling, H., Edge, A. C., Fabian, A. C., Allen, S. W., Crawford, C. S., & Boehringer, H. 1997, *ApJ*, 479, L101
- Efstathiou, G., Bond, J. R., & White, S. D. M. 1992, *MNRAS*, 258, 1P
- Eke, V. R., Cole, S., & Frenk, C. S. 1996, *MNRAS*, 282, 263
- Ellingson, E., Yee, H. K. C., Abraham, R. G., Morris, S. L., & Carlberg, R. G. 1998, *ApJS*, 116, 247
- Ellingson, E., Yee, H. K. C., Abraham, R. G., Morris, S. L., Carlberg, R. G., & Smecker-Hane, T. A. 1997, *ApJS*, 113, 1
- Feigelson, E. D. & Nelson, P. I. 1985, *ApJ*, 293, 192
- Fritsch, G. & Bheuhert, T. 1999, *A&A*, 344, 759
- Gal, R. R., DeCarvalho, R. R., Odewahn, S. C., Djorgovsky, S. G., & Margoniner, V. E. 2000, *AJ*, 119, accepted
- Gioia, I. M., Henry, J. P., Maccacaro, T., Morris, S. L., Stocke, J. T., & Wolter, A. 1990a, *ApJ*, 356, 35
- Gioia, I. M., Maccacaro, T., Schild, R. E., Wolter, A., Stocke, J. T., Morris, S. L., & Henry, J. P. 1990b, *ApJS*, 72, 567
- Girardi, M., Borgani, S., Giuliano, G., Mardirossian, F., & Mezzetti, M. 1998, *ApJ*, 506, 45
- Henry, J. P. 1997, *ApJ*, 489, L1
- Henry, J. P., Gioia, L., Maccacaro, T., Morris, S. L., Stocke, J., & Wolter, A. 1992, *ApJ*, 386, 408
- Hogg, D. 1999
- Holden, B. P., Nichol, R. C., Romer, A. K., Metevier, A., Postman, M., Ulmer, M. P., & Lubin, L. M. 1999, *AJ*, 118, in press
- Holden, B. P., Romer, A. K., Nichol, R. C., & Ulmer, M. P. 1997, *AJ*, 114, 567
- Jones, C. & Forman, W. 1992, in *Clusters and Superclusters of Galaxies*, ed. A. C. Fabian (Dordrecht: Kluwer), 49
- Katgert, P., Mazure, A., Perea, J., Den Hartog, R., Moles, M., Le Fevre, O., Dubath, P., Focardi, P., Rhee, G., Jones, B., Escalera, E., Biviano, A., Gerbal, D., & Giuricin, G. 1996, *A&A*, 310, 8
- Kepner, J., Fan, X., Bahcall, N., Gunn, J., Lupton, R., & Xu, G. 1999, *ApJ*, 517, 78

- Kitayama, T. & Suto, Y. 1997, *ApJ*, 490, 557
- Kurtz, M. & Mink, D. 1998, *PASP*, 110, 934
- Lacey, C. & Cole, S. 1993, *MNRAS*, 262, 627
- Lubin, L. 1996, *AJ*, 112, 23
- Marshall, H. L., Tanabaum, H., Avni, Y., & Zamorani, G. 1983, *ApJ*, 269, 35
- Mazure, A., Katgert, P., Den Hartog, R., Biviano, A., Dubath, P., Escalera, E., Focardi, P., Gerbal, D., Giuricin, G., Jones, B., Le Fevre, O., Moles, M., Perea, J., & Rhee, G. 1996, *A&A*, 310, 31
- Miller, C. J., Merlott, A. L., & C., N. R. 2000, *ApJ*, submitted
- Morrison, R. & McCammon, D. 1983, *ApJ*, 270, 119
- Nichol, R. C., Holden, B. P., Romer, A. K., Ulmer, M. P., Burke, D. J., & Collins, C. A. 1997, *ApJ*, 481, 644
- Nichol, R. C., Romer, A. K., Holden, B. P., Ulmer, M. P., Pildis, R. A., Adami, C., Merrelli, A. J., Burke, D. J., & Collins, C. A. 1999, *ApJ*, 521, L21
- Nichol, R. C., Ulmer, M. P., Kron, R. G., Wirth, G., & Koo, D. C. 1994, *ApJ*, 432, 464
- Olsen, L. F., Scodreggio, M., Da Costa, L., Benoist, C., Bertin, E., Deul, E., Erben, T., Guarnieri, M. D., Hook, R., Nonino, M., Prandoni, I., Slijkhuis, R., Wicenec, A., & Wichmann, R. 1999, *A&A*, 345, 681
- Poggianti, M. 1997, *A&AS*, 122, 399
- Postman, M. P., Lubin, L. M., Gunn, J. E., Oke, J. B., Hoessel, J. G., Schneider, D. P., & Christensen, J. A. 1996, *AJ*, 111, 615
- Press, W. H. & Schechter, P. 1974, *ApJ*, 187, 425
- Reichart, D. E., Castander, F. J., & Nichol, R. C. 1999a, *ApJ*, 516, 1
- Reichart, D. E., Nichol, R. C., Castander, F. J., Burke, D. J., Romer, A. K., Holden, B. P., Collins, C. A., & Ulmer, M. P. 1999b, *ApJ*, 518, 521
- Romer, A. K., Nichol, R. C., Holden, B. P., Ulmer, M. P., Pildis, R. A., Merrelli, A., Adami, C., Burke, D. J., Collins, C. A., Metevier, A. J., Kron, R. G., & Commons, K. 2000, *ApJS*, in press
- Rosati, P., Della Ceca, R., Norman, C., & Giacconi, R. 1998, *ApJ*, 492, L21
- Schmitt, J. H. M. M. 1985, *ApJ*, 293, 178

- Stark, A. A., Gammie, C. F., Wilson, R. W., Balley, J., Linke, R. A., Heiles, C., & Hurwity, M. 1992, ApJS, 79, 77
- Viana, P. T. P. & Liddle, A. R. 1996, MNRAS, 281, 323
- Victoria Alonso, M., Valotto, C., Lambdas, D. G., & Muriel, H. 1999, MNRAS, 308, 618
- White, R. A., Bliton, M., Bhavsar, S., Bornmann, P., Burns, J. O., Ledlow, M., & Loken, C. 1999, in American Astronomical Society Meeting, Vol. 194, 8804
- Yee, H. K. C., Ellingson, E., Morris, S. L., Abraham, R. G., & Carlberg, R. G. 1998, ApJS, 116, 211

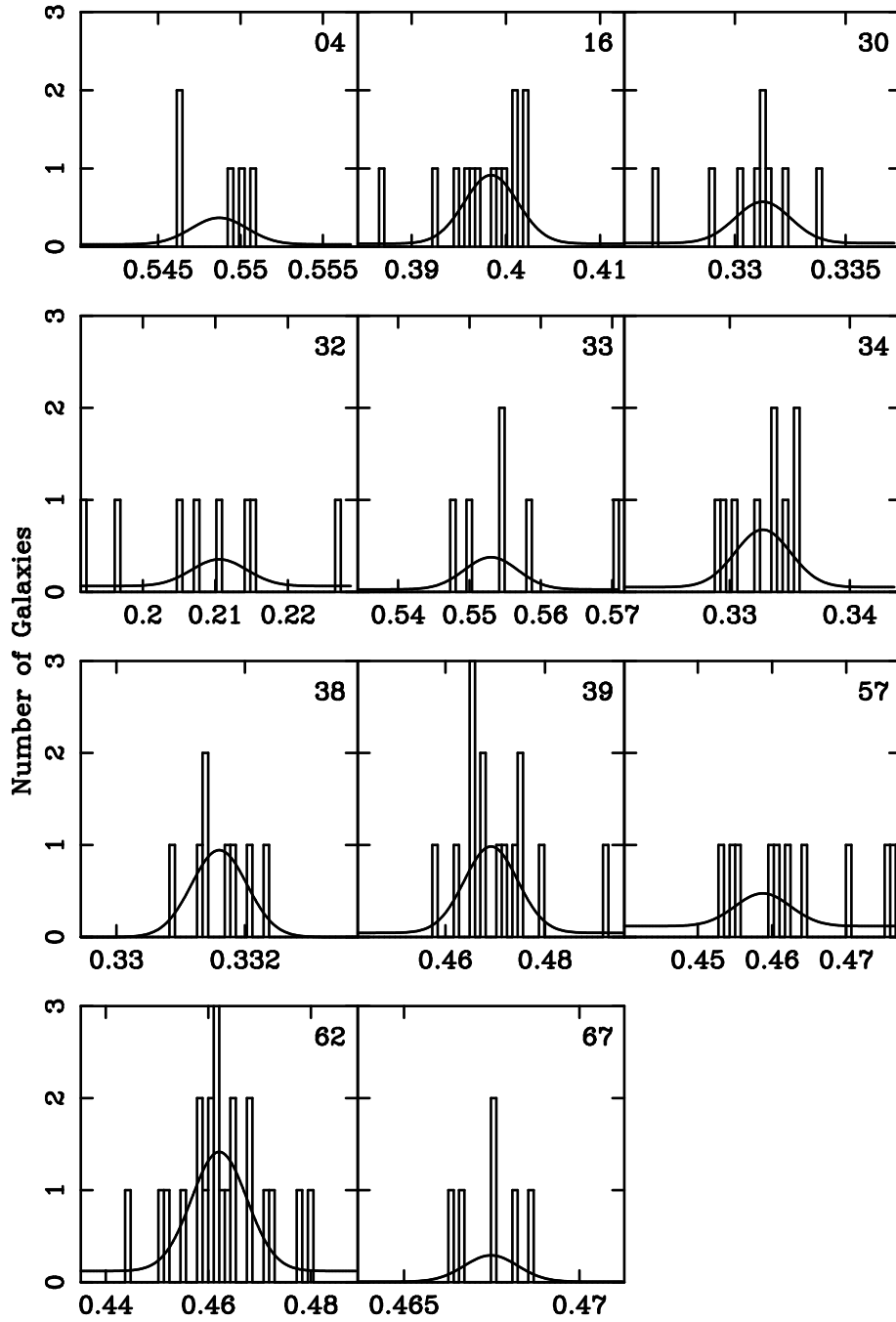


Fig. 1.— Redshift distributions of PDCS clusters in CFHT sample. The histograms contain all redshifts within $5\sigma_v$ of the mean of the CFHT data. The solid line is the Gaussian plus fit to the redshift data.

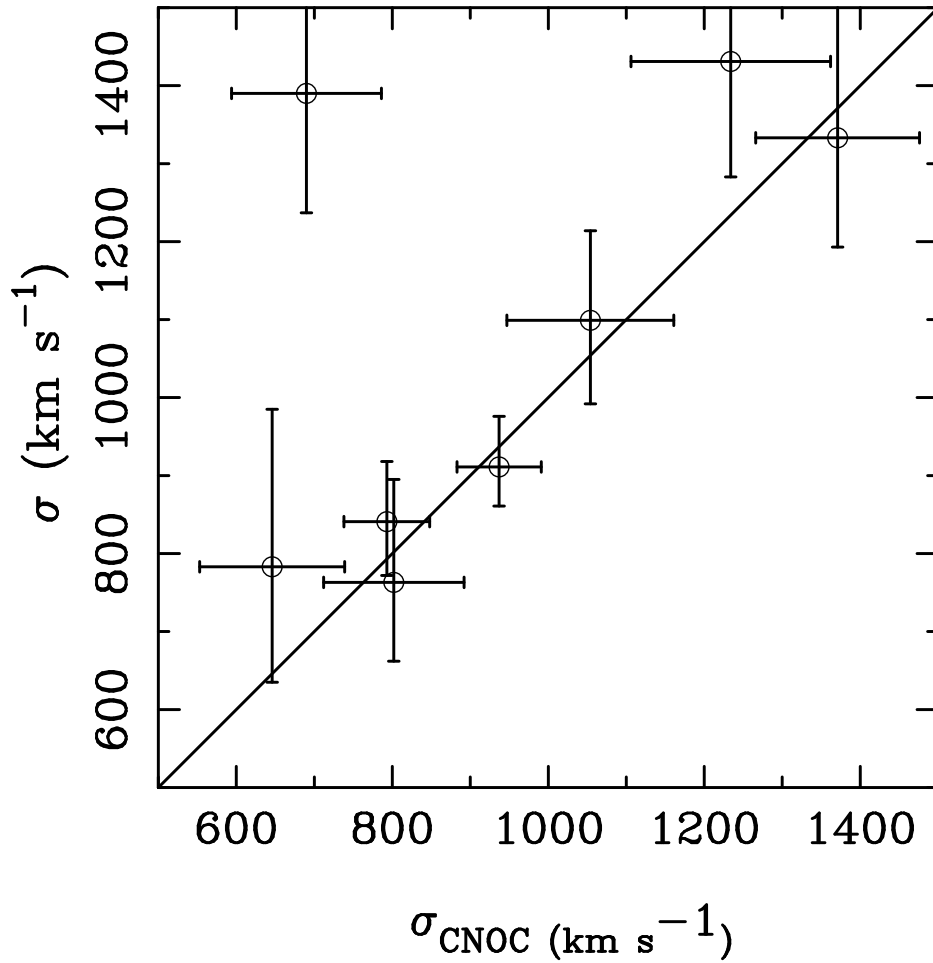


Fig. 2.— Comparison of velocity dispersion estimates for the CNOC clusters. The x-axis are those estimates from Carlberg *et al.* (1996) while the y-axis are the estimates based on the maximum likelihood technique discussed in this work. We also plot a 45° line. The point in strong disagreement with the 45° line is MS1512+36.

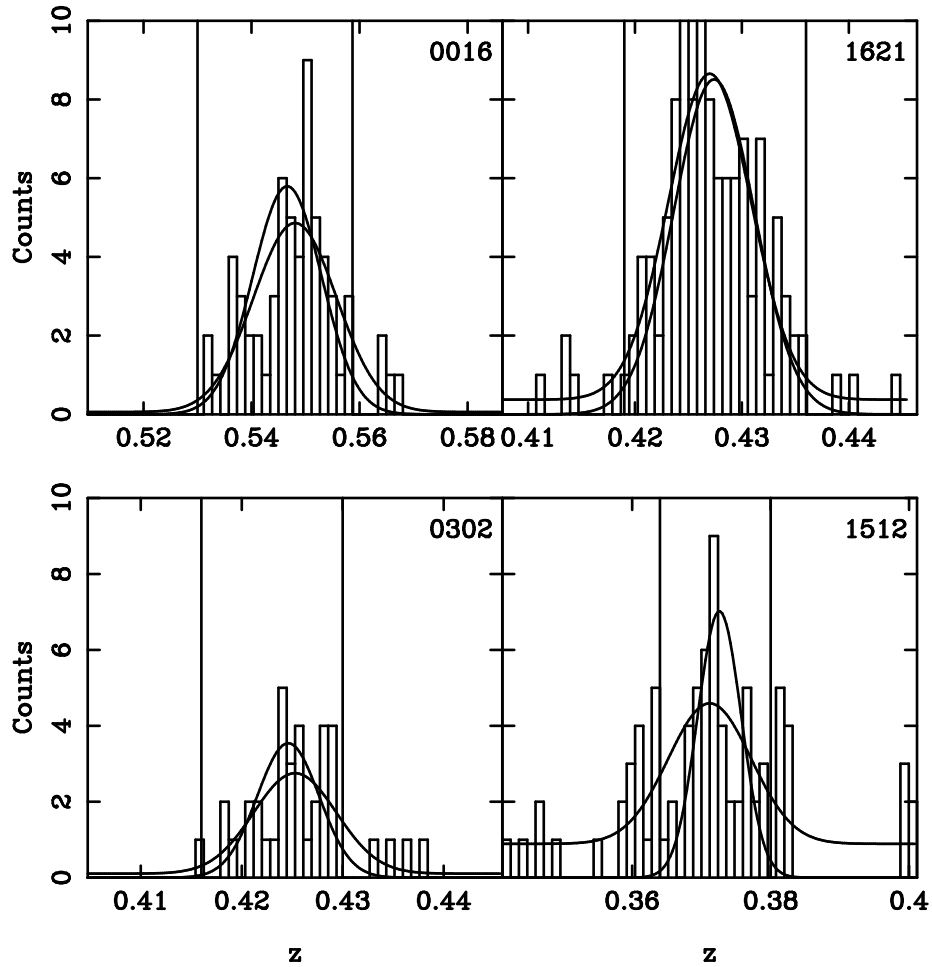


Fig. 3.— Redshift distributions of four CNOC clusters with velocity dispersions. The histograms contain all redshifts within $5\sigma_v$ of the mean. The solid line with a background is the estimate from above. The solid line originating from the x-axis is the estimate from Carlberg et al. (1996). The two solid vertical lines represent the range in redshift used by Carlberg et al. (1996) for estimating the velocity dispersion. The bottom two histograms are of the two clusters that our estimate has the largest deviation from the CNOC estimate.

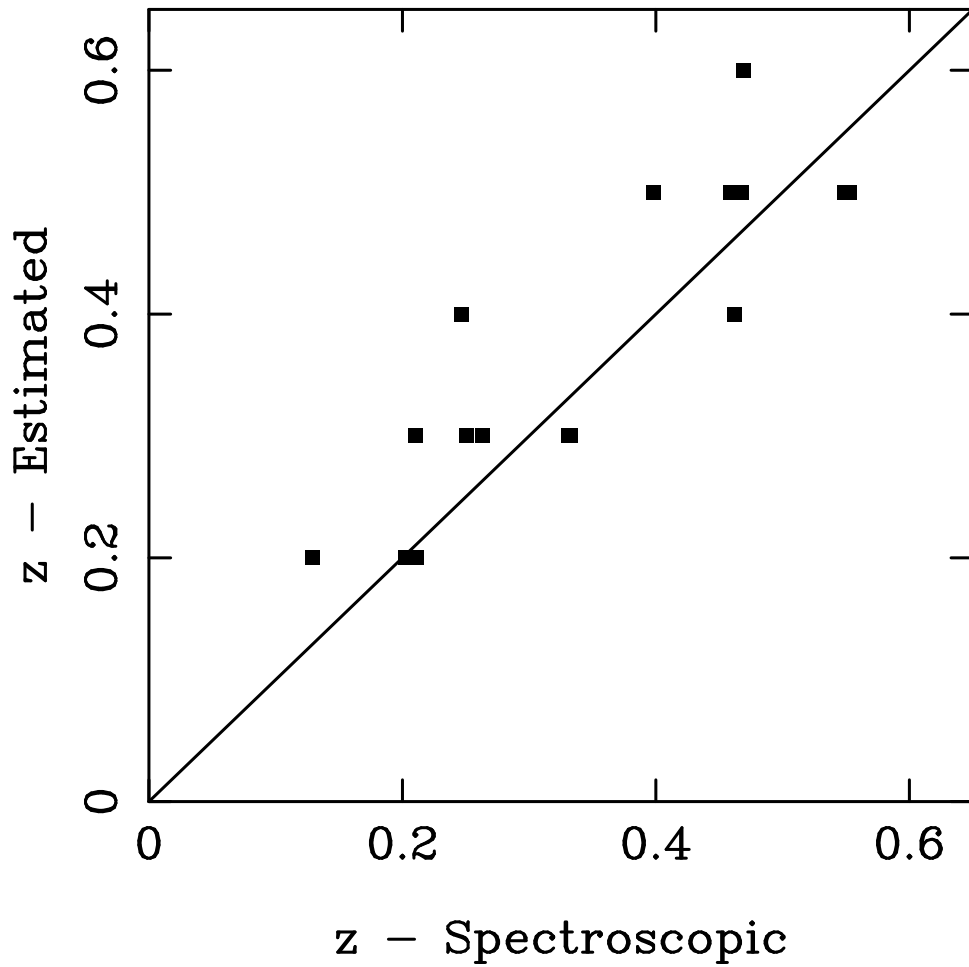


Fig. 4.— Measured redshifts compared match-filter estimated redshifts. We plot the PDCS estimated redshifts as a function of spectroscopically measured redshifts for both the CFHT and the ARC/KPNO sample. We also plot a 45° line, not a fit, for comparison.

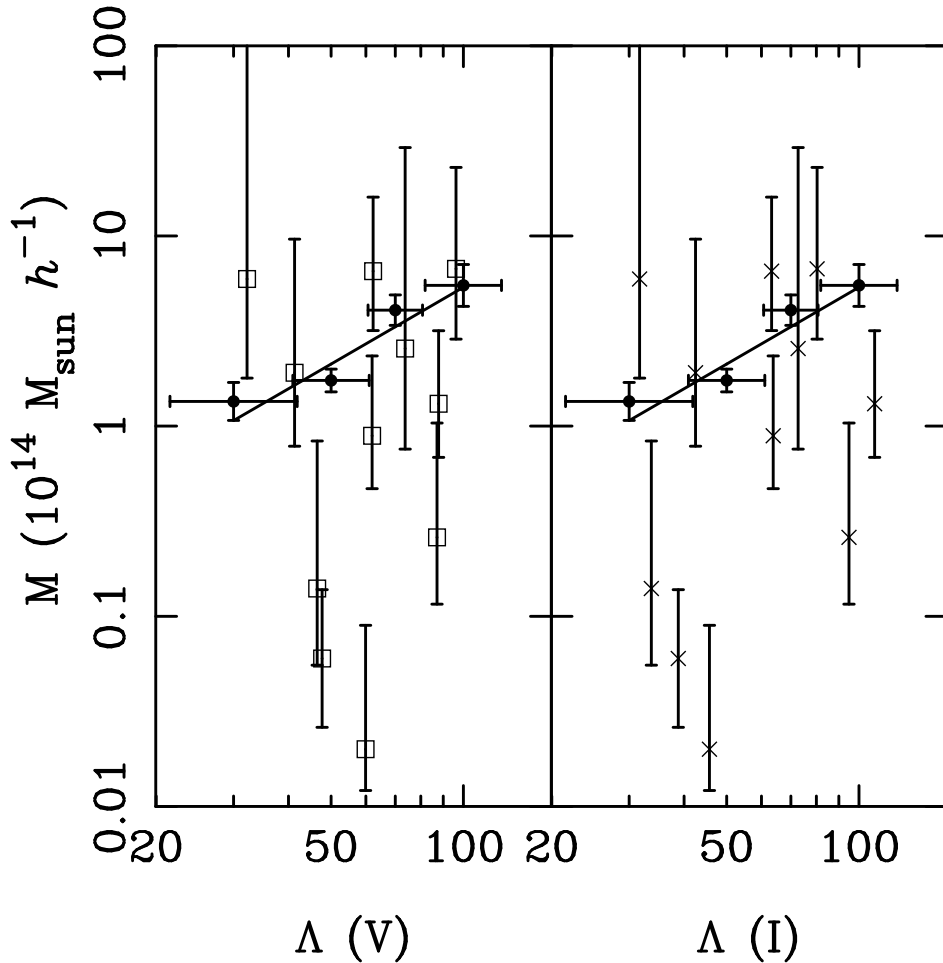


Fig. 5.— Mass as a function of richness. We use the mass from equation (1) and the PDCS Λ richness. The V band richness is plotted with open squares in the left panel while the I band richness is plotted with crosses in the right panel. Also, we plot the mass-richness relation from Girardi *et al.* (1998a). That relation is plotted using solid circles. The vertical error bars represent the scatter around the mean of the sample at that Richness Class. The x-axis error bars represent the range in PDCS richness for the Richness Class. The Richness Classes in this plot are (from left to right) 0, 1, 2, and ≥ 3 . We plot, as a line, our fit to the Girardi *et al.* (1998a) richness-mass relation.

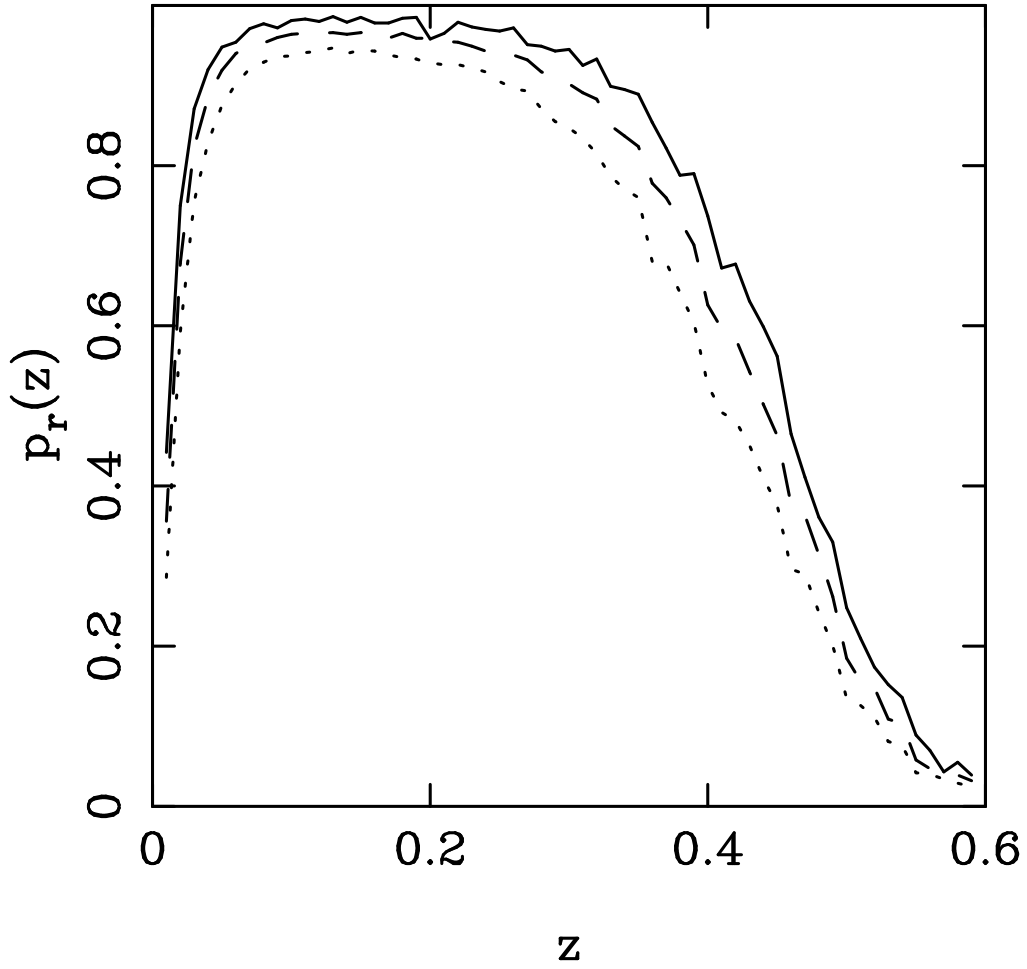


Fig. 6.— Probability of successfully measuring a redshift for the ARC/KPNO sample as a function of redshift. The three lines are for Richness Class 3 (solid), Richness Class 2 (dashed) and Richness Class 1 (dotted).

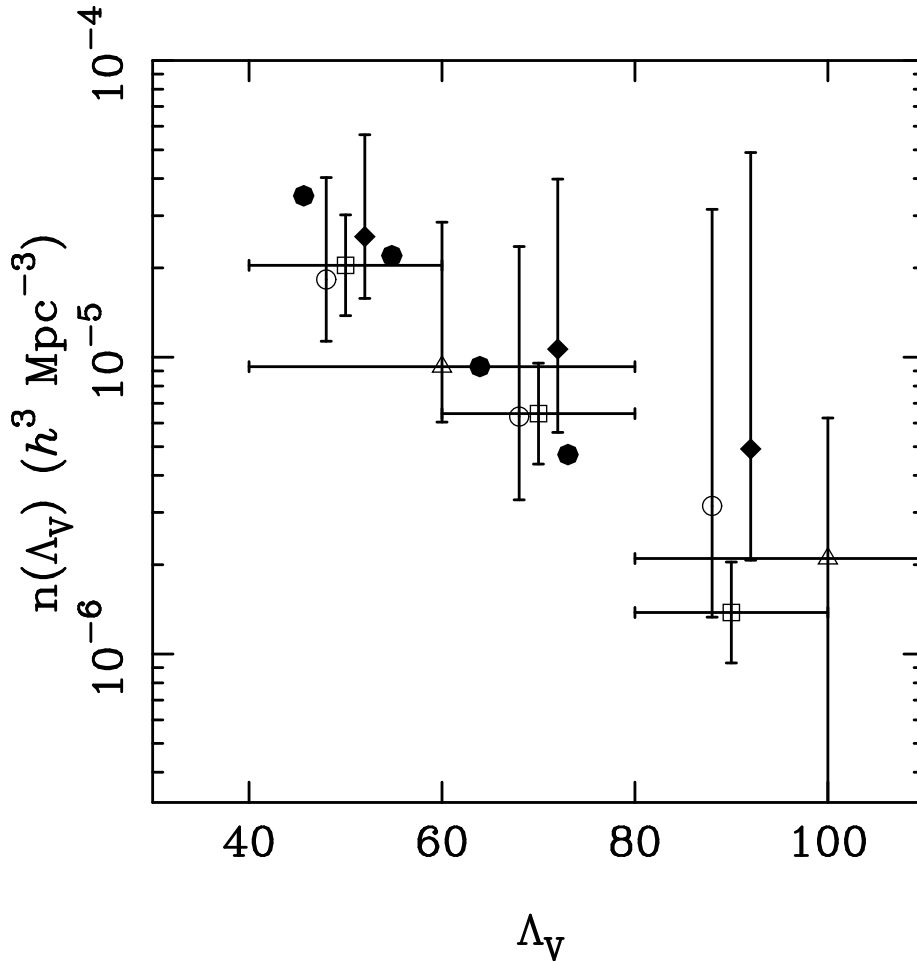


Fig. 7.— Space density as a function of Richness for the PDCS clusters in the original catalog (open squares), from the ARC/KPNO sample (solid diamonds), and from the CFHT sample (open circles). The vertical error bars are the 68% confidence limits for a Poisson distribution from Gehrels (1986). The open triangles represent the results from Table 2 of Bramel *et al.* (2000). We also plot with solid circles the space density from the APM cluster catalog. The error bars for the original catalog are as given in Postman *et al.* (1996). The horizontal error bars give the range in Richness covered by the different Richness Classes. We note here that Bramel *et al.* (2000) use a different relation between Λ and Abell Richness Class.

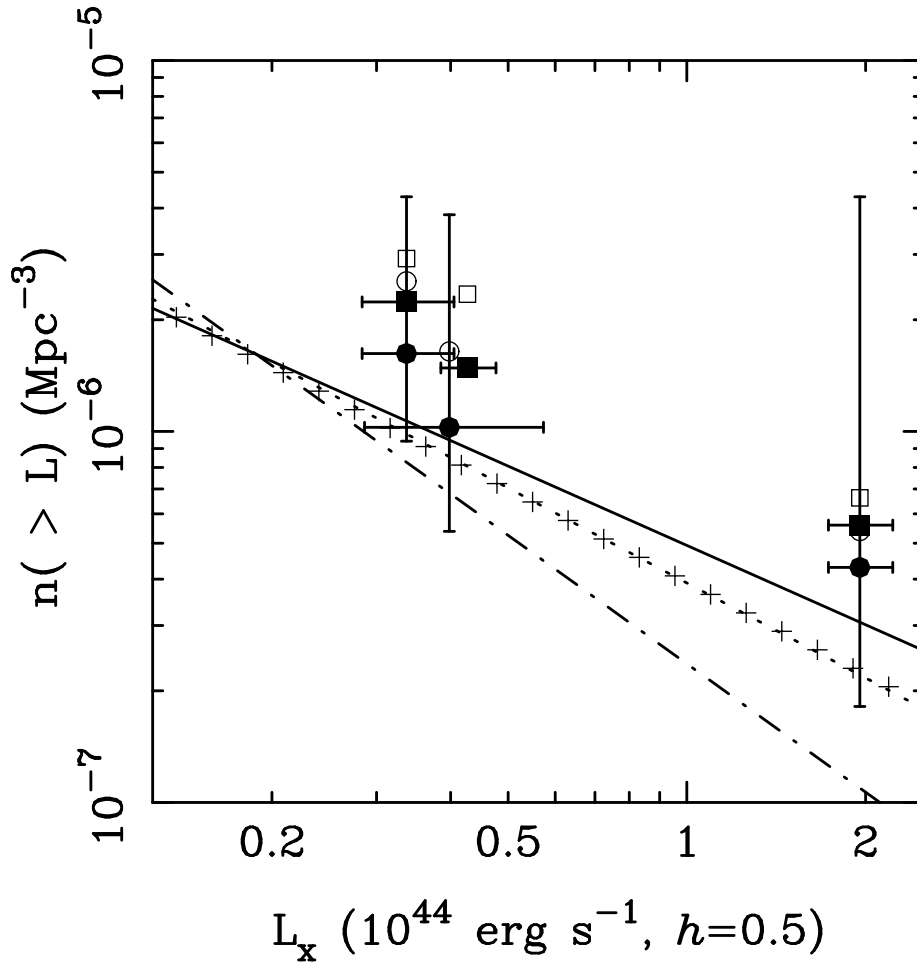


Fig. 8.— Cumulative X-ray luminosity function of PDCS clusters in the CFHT sample using both the detections (solid circles) and upper limits (open circles). Our results from the ARC/KPNO sample are plotted using squares with solid representing the detections and open representing the combination of detections and upper limits. We plot the parametric distributions from Burns *et al.* (1996) (solid line), Ebeling *et al.* (1997) (dotted line), Burke *et al.* (1997) (dot-dashed line) & Rosati *et al.* (1998) (+ symbols). The error bars are for a Poisson distribution at each point in the cumulative distribution of detections. The luminosity errors are 68% confidence limits from Table 5.

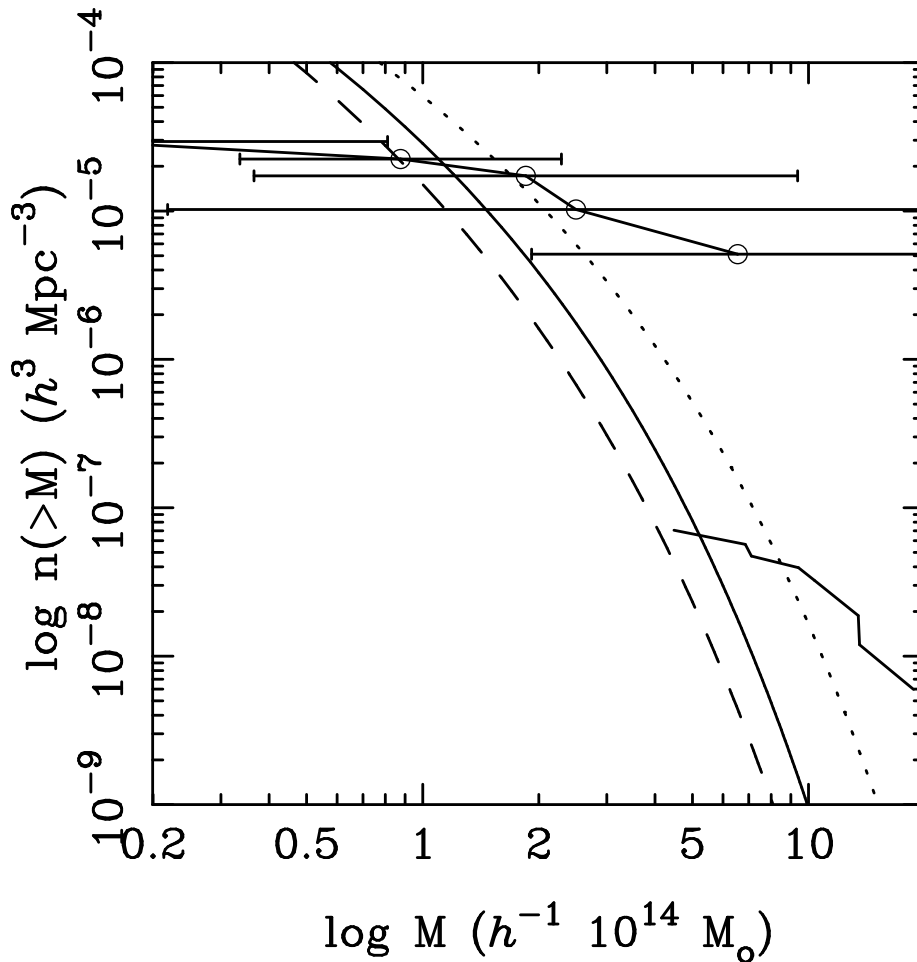


Fig. 9.— Cumulative space density of PDCS clusters as a function of mass from the CFHT sample. The points with error bars represents our cumulative distribution function. The solid curve the lower right is the cumulative mass distribution for the CNOC cluster survey. The smooth solid line represents the best fit from Bahcall, Fan, & Cen (1997), the dashed line is from Carlberg *et al.* (1997), a fit to the CNOC cluster sample, and the dotted line is the $\Omega_m = 0.32$ and $\sigma_8 = 0.97$ line from the text. All of the theoretical mass functions are calculated for a redshift of 0.4, the mean of the range of allowed redshifts. The volumes for the CNOC and PDCS mass functions are computed for $q_o = 0.16$.

Table 1. PDCS Cluster Candidates X-ray Data: Observed Quantities.

PDCS # ^a	α (J2000)	δ (J2000)	z^b	Aper. ^c	Time (s)	Cts	Background Cts	Fraction ^d
01	00 29 03.0	+05 01 24	0.600	2'56	4224.0	35	20.7	0.80
02	00 29 28.4	+05 04 03	0.246	4'17	4897.4	82	76.5	0.80
03	00 28 36.6	+05 07 44	0.600	2'42	5465.8	31	29.7	0.80
04	00 29 11.1	+05 08 55	0.549	2'76	4660.1	11	11.2	0.53
05	00 27 38.6	+05 09 46	0.211	4'28	6328.5	86	84.0	0.79
06	00 29 52.2	+05 12 36	0.400	3'98	4333.9	75	59.7	0.80
08	00 28 31.4	+05 18 01	0.600	2'50	3666.4	22	25.9	0.76
29	09 53 12.1	+47 08 58	0.400	3'18	17183.2	194	196.6	0.80
30	09 54 46.3	+47 10 48	0.259	4'19	14210.8	290	269.6	0.78
31	09 53 39.5	+47 12 58	1.100	2'26	17687.0	120	90.6	0.80
32	09 52 29.0	+47 17 49	0.211	4'33	18326.3	328	300.0	0.77
33*	09 52 13.1	+47 16 48	0.553	2'57	17446.5	107	77.2	0.69
34	09 55 09.1	+47 29 55	0.333	3'39	12202.6	211	193.4	0.80
35	09 52 31.2	+47 36 27	0.600	2'36	17409.9	125	102.0	0.80
36*	09 53 53.7	+47 40 15	0.251	3'80	14564.7	369	261.6	0.80
37	09 51 41.5	+47 41 30	0.600	2'43	14651.7	117	90.8	0.80
38	09 51 09.9	+47 43 54	0.332	3'34	14432.2	154	159.4	0.80
39	09 51 25.2	+47 49 50	0.469	2'91	11528.6	113	127.0	0.80
40*	09 53 25.6	+47 58 55	0.203	4'63	10704.2	331	161.3	0.76
41*	09 54 16.9	+47 58 41	0.700	2'98	9667.9	102	71.6	0.77
42	09 53 54.2	+48 00 04	0.900	2'82	9401.2	60	51.3	0.72
43	09 52 15.1	+47 57 44	0.200	4'65	11699.9	279	259.1	0.78
44	09 52 18.6	+48 02 32	1.100	2'92	9925.8	76	91.2	0.78
45*	09 54 38.8	+47 15 59	0.400	3'18	15273.1	228	161.4	0.79

Table 1. PDCS Cluster Candidates X-ray Data: Observed Quantities.

PDCS # ^a	α (J2000)	δ (J2000)	z^b	Aper. ^c	Time (s)	Cts	Background Cts	Fraction ^d
57	13 23 47.3	+30 03 31	0.459	3'85	15357.7	363	331.2	0.80
59	13 24 48.8	+30 11 36	0.751	2'51	16828.8	160	152.0	0.80
60	13 23 39.0	+30 12 12	0.200	4'71	14693.9	408	502.7	0.80
61	13 27 07.4	+30 18 01	0.300	4'41	13924.4	252	243.3	0.72
62*	13 23 39.0	+30 22 26	0.462	2'82	15467.2	345	196.2	0.80
63*	13 24 20.6	+30 12 52	0.697	2'53	16252.9	209	121.2	0.80
64	13 26 22.3	+30 15 20	1.000	2'79	19129.5	177	151.3	0.80

^aThe PDCS identification number, clusters marked with an * are X-ray detections.

^bRedshift used to compute the aperture size

^cAperture that contains 80% of the total flux for the model specified in the text

^dThe fraction of the model total flux expected to fall within the aperture.

Table 2. PDCS Candidates in CFHT Sample.

PDCS #	α (J2000.0)	δ (J2000.0)	$z_{estimated}^a$	Λ_V^a	# of Masks ^b	z range ^c
04	00 29 11.1	+05 08 55	0.5	87.1	2	0.43-0.61
16	02 28 26.5	+00 32 20	0.5	87.8	2	0.43-0.61
30	09 54 46.3	+47 10 48	0.3	46.5	2	0.20-0.56
32	09 52 29.0	+47 17 49	0.3	32.2	in 33	0.43-0.61
33	09 52 13.1	+47 16 48	0.5	41.3	2	0.43-0.61
34	09 55 06.1	+47 29 56	0.3	62.0	2	0.20-0.56
38	09 51 09.9	+47 43 55	0.3	47.7	2	0.20-0.56
39	09 51 25.2	+47 49 50	0.6	62.3	in 38	0.20-0.56
45	09 53 48.4	+47 57 57	0.4	36.6	in 30	0.20-0.56
57	13 23 47.9	+30 03 24	0.5	73.7	2	0.43-0.61
61	13 27 02.4	+30 18 14	0.3	33.2	1	0.20-0.56
62	13 23 42.2	+30 22 38	0.4	96.2	2	0.43-0.61
67	16 93 49.4	+41 11 13	0.5	59.9	1	0.43-0.61

^a Column four lists the estimated redshift and column five lists the richness which were used to select clusters for the observation.

^bThe number masks used for measuring redshift of cluster members. If a cluster is noted as “in #”, that cluster was observed using the masks for another PDCS cluster. The number specifies which cluster that is.

^cThe redshift ranges of the blocking filter used, see Adami *et al.* 2000 for how these ranges were determined.

Table 3. PDCS cluster redshifts for clusters only in ARC/KPNO sample

PDCS #	z^a	# of galaxies ^b	Λ_V	$z_{estimated}$
02	0.2463	3/7	44.4	0.4
05	0.2112	3/3	31.8	0.2
12	0.2634	6/8	75.5	0.3
23	0.1288	6/7	43.6	0.2
36	0.2505	4/6	54.7	0.3
40	0.2028	5/5	28.3	0.2

^a“Best” redshift from Holden *et al.* 1999.

^bFraction of total redshifts observed within 1500 km s⁻¹ of the “best” redshift.

Table 4. Redshifts and Velocity Dispersions of CFHT sample.

PDCS #	$z_{\text{biweight}}^{\text{a}}$	$\sigma_{v,\text{biweight,obs}}^{\text{a}}$	$\sigma_{v,\text{biweight,rest}}^{\text{a,b}}$ (km s ⁻¹)	z_{ML}^{c}	$\sigma_{v,\text{ML,obs}}^{\text{c}}$	$\sigma_{v,\text{ML,rest}}^{\text{b,c}}$ (km s ⁻¹)
04	0.5486	0.002288	443	0.5486	0.001900	368 ⁺¹⁶⁹ ₋₉₇
16	0.3984	0.003149	675	0.3984	0.002820	604 ⁺¹⁷⁸ ₋₁₃₀
30	0.3311	0.001957	441	0.3314	0.000515	280 ⁺¹⁶⁷ ₋₈₈
32	0.2106	0.004507	1111	0.2105	0.003824	947 ⁺¹⁶⁷ ₋₈₈
33	0.5530	0.004414	852	0.5530	0.003689	712 ⁺³⁸⁵ ₋₂₁₂
34	0.3327	0.002322	522 ⁺¹⁶⁷ ₋₁₁₂
38	0.3316	0.001169	263	0.3322	0.000444	101 ⁺²⁸ ₋₂₄
39	0.4691	0.006063	1237	0.4692	0.005149	1051 ⁺³¹⁴ ₋₂₅₂
57	0.4586	0.004274	878	0.4588	0.003730	767 ⁺⁶²⁸ ₋₂₇₁
62	0.4619	0.005858	1201	0.4621	0.005162	1059 ⁺⁴³⁴ ₋₃₀₀
67	0.4675	0.000896	183	0.4675	0.000760	155 ⁺⁶⁸ ₋₃₁

^a The values noted by biweight are derived from the first pass through the data.

^b For both the maximum likelihood fits and the biweight estimators, we give the rest-frame velocity dispersion in km s⁻¹.

^c The values noted by ML are from the maximum likelihood fits of a Gaussian plus flat background galaxy distribution.

Table 5. PDCS Cluster Candidate X-ray Data: Physical Quantities

PDCS # ^a	Flux ^b (10^{-14} erg s ⁻¹ cm ⁻²)	Luminosity ^b (10^{43} erg s ⁻¹)
01	5.4	2.4
02	9.7	0.7
03	5.4	2.5
04	6.0	2.3
05	7.7	0.4
06	9.3	1.8
08	6.0	2.7
29	4.1	0.8
30	5.5	0.4
31	2.6	4.4
32	4.8	0.2
33*	$3.1^{+1.1}_{-1.0}$	$1.2^{+0.4}_{-0.4}$
34	5.3	0.7
35	2.9	1.3
36*	$12.5^{+2.3}_{-2.2}$	$0.9^{+0.2}_{-0.2}$
37	3.1	1.4
38	4.3	0.6
39	4.4	1.2
40*	$24.1^{+2.7}_{-2.5}$	$1.1^{+0.1}_{-0.1}$
41*	$4.3^{+1.5}_{-1.3}$	$2.7^{+0.9}_{-0.8}$
42	3.7	4.0
43	7.0	0.3
44	5.0	8.3
45*	$6.2^{+1.5}_{-1.4}$	$1.2^{+0.3}_{-0.3}$

Table 5. PDCS Cluster Candidate X-ray Data: Physical Quantities

PDCS # ^a	Flux ^b (10^{-14} erg s ⁻¹ cm ⁻²)	Luminosity ^b (10^{43} erg s ⁻¹)
57	5.7	1.5
59	3.3	2.4
60	6.4	0.3
61	5.1	0.5
62*	$21.5^{+2.8}_{-2.6}$	$5.6^{+0.7}_{-0.7}$
63*	$8.7^{+1.5}_{-1.4}$	$5.4^{+0.9}_{-0.9}$
64	3.2	4.4

^aClusters marked with a * are considered detections.

^bErrors are given only for detections, values without errors are 3σ upper limits.

Table 6. Fractional Change of Survey Volume from Model Variations.

Parameter Changed	Percent Change in Volume
q_o increased to 0.5	-22%
$3 \times r_c$	-11%
$\frac{1}{3} \times r_c$	+11%
$\Delta M_\star = +0.1$	-9%
$\Delta M_\star = -0.1$	+0.2%
Sbc K corrections	+40%
Poggianti K corrections	-10%

Table 7. Richness Function for ARC/KPNO and CFHT Samples.

Sample ^a	Richness Class 1 ^b $40 \leq \Lambda \leq 60$ $10^{-6} h^3 \text{ Mpc}^{-3}$	Richness Class 2 ^b $60 \leq \Lambda \leq 80$ $10^{-6} h^3 \text{ Mpc}^{-3}$	Richness Class 3 ^b $80 \leq \Lambda \leq 120$ $10^{-6} h^3 \text{ Mpc}^{-3}$
ARC/KPNO – V	$25.5^{+20.2}_{-12.2}$ (4)	$10.7^{+14.1}_{-6.9}$ (2)	$4.9^{+11.3}_{-4.2}$ (1)
ARC/KPNO – I	$12.7^{+16.8}_{-8.2}$ (2)	$10.7^{+14.1}_{-6.9}$ (2)	$4.9^{+11.3}_{-4.2}$ (1)
CFHT – V	$18.3^{+14.5}_{-8.8}$ (4)	$6.3^{+8.3}_{-4.1}$ (2)	$3.2^{+7.4}_{-2.8}$ (1)
CFHT – I	$9.1^{+7.2}_{-5.9}$ (2)	$6.3^{+8.3}_{-4.1}$ (2)	$3.2^{+7.4}_{-2.8}$ (1)

^aThe four samples in this table are defined by the two different selection processes from Sec. 4.2 and 4.3, and by using the V and I band richnesses to determine the Richness Classes.

^bThe value in parentheses is the number of clusters from the sample in that Richness Class, as defined by Λ . The volumes are listed in Sec. 4.2 and 4.3. We list the 68% confidence limits based on a Poisson distribution using the values from Gehrels 1986.